SERI/STR-211-2556
(DE85008775)
Distribution Category UC-63

Research on Electrochemical Photovoltaic Cells

Final Report
1 July 1982 - 30 April 1983

A Subcontract Report

D. Tench, Principal Investigator
Rockwell International Science Center
Thousand Oaks, California

March 1985

Prepared under Subcontract No. XE-2-02126-1

SERI Technical Monitor: W. Wallace

Solar Energy Research Institute
A Division of Midwest Research Institute

1617 Cole Boulevard
Golden, Colorado 80401

Prepared for the
U.S. Department of Energy
Contract No. DE-AC02-83CH10093

TABLE OF CONTENTS

LIST OF FIGURES

LIST OF TABLES

1.0 ABSTRACT

The overall goal of this program is to provide the basis for designing a practical electrochemical solar cell based on the II-VI compound semiconductors. Emphasis is on developing new solvent/redox systems and conducting films which will stabilize the II-VI compounds against photodissolution without seriously degrading the long-term solar response, and on applying electrochemical photocapacitance spectroscopy (EPS) to the development of improved thin-film materials.

For photoelectrode stabilization, work was focused on electrodeposited polypyrrole. A principal thrust in this area was to determine the effects of the deposition parameters on the film density and electrical conductivity, which are critical to the performance of the film as an effective barrier to ionic transport without appreciable degradation of the cell performance. These film properties are found to vary dramatically with the substrate, deposition conditions, electrolyte and anion employed, which indicates that there is considerable leeway for improvement. To date, the most dense and highly conductive films have involved polymeric anions, nonaqueous solvents, and metallic substrates. A promising approach to providing an improved surface for polymer deposition on semiconductors, i.e., controlled chemical deposition of metals from solution, has also been identified.

In the EPS area, some effort was devoted to establishing the quantitative aspects of the method and obtaining preliminary results for thin-film p-Zn_3P_2 and a-Si, but the focus was on the development of thin-film CdSe materials, in collaboration with Grumman Aerospace. The previously-detected 0.2 eV interface state, which has been observed in appreciable concentrations only for CdSe films prepared at low substrate temperatures, was conclusively shown to mediate electron exchange between the semiconductor and polysulfide species in solution. To further elucidate the role of this state in charge transfer processes, steady-state and transient EPS studies and ac impedance measurements over a wide frequency range were performed for a variety of

materials as a function of electrode potential. The results identify the 0.2 eV state as an effective charge carrier recombination center. Considerable variation in the concentration of this interface state from electrode to electrode, even within the same batch, was observed, indicating considerable room for improvement in the deposition process.

2.0 PROJECT DESCRIPTION

During the past several years, SERI has funded a broad photoelectrochemical cell program in which the Rockwell role has evolved toward investigation/development of surface films for stabilization of semiconductor photoanodes and application of electrochemical photocapacitance spectroscopy (EPS) to the development of thin film semiconductor materials. The focus on protective films is based on considerable experience with redox electrolytes, both aqueous and nonaqueous, which indicates that improvement in the conversion efficiency, compared to that offered by the aqueous sulfide/polysulfide system (5-6%), will require an alternate means of protecting the semiconductor from photodegradation. A significant Rockwell accomplishment was the demonstration that high open circuit voltages, and thus high conversion efficiencies, are attainable for polymer film-covered electrodes in various electrolytes [1-3], e.g., $Fe^{3+/2+}$ in aqueous and nonaqueous solvents. This work has been extended and improved upon in various laboratories [4-9], but stabilization adequate for a practical device has not been attained, apparently because of excessive porosity of the film materials investigated (polypyrrole and polyaniline) which permits slow degradation of the film-semiconductor interface and loss of film adhesion. Improved film materials are needed.

The electrochemical photocapacitance spectroscopy (EPS) method [10], developed under this program, has been demonstrated to be a powerful new tool for characterization of a wide variety of single crystal and polycrystalline semiconductor materials, including GaAs, GaP, Zn_3P_2, a-Si and the cadmium chalcogenides. Both bulk and interface states, which can be distinguished from the bias potential dependence of the corresponding capacitance changes, have been detected and excellent correlations have been established between the energies and densities of states determined by EPS and those obtained by solid-state measurements, both in-house and reported in the literature. It has also been demonstrated that photocapacitance transient measurements yield quantitative information concerning the state population/depopulation kinetics. Under the present program, EPS is being applied to the development of

improved thin-film photovoltaic materials. This work is a co-operative effort involving other SERI contractors and is focused on n-CdSe and mixed chalcogenides.

3.0 TECHNICAL PROGRESS DESCRIPTION

3.1 Protective Films

Our approach in the protective film area has been to investigate both alternate film materials and modifications of existing films. Other workers have reported some success with platinum silicide [11] and indium tin oxide [12,13], but these materials tend to pin the semiconductor Fermi level, limiting the attainable photovoltages. During the past year, more encouraging results have been reported for "intrinsic" oxides. In particular, Lewis and coworkers [14,15] found that n-$GaAs_{1-x}P_x$ and n-Si photoanodes with conversion efficiencies in the 10-13% range are stabilized by thin oxide films in rigorously dried nonaqueous electrolytes. Similar results were reported for single crystal InP in aqueous acidic electrolytes [16]; the other III-V semiconductors apparently do not form analogous coherent oxide films. In keeping with our overall emphasis on electrodeposition for film preparation, we investigated electrodeposited oxide films [17] but found that the porosity was generally too high to afford long-term protection of narrow-bandgap semiconductor electrodes. Consequently, our current efforts are focused on polymer films, for which Fermi level pinning does not appear to be a problem and considerable flexibility exists for structural modifications.

Recently, under an associated contract with the Navy, we have prepared free-standing polypyrrole films, for which the important film properties can be determined. The film density, and thus the porosity, as well as the electrical conductivity were found to vary dramatically with the electrolyte used for deposition. Tables 1-3 give the film preparation conditions, composition and physical properties, respectively. Films were deposited on a 28 cm^2 flat gold-plated copper disc from unstirred solutions with a cylindrical platinum gauze cathode directly above the anode. The following conclusions can be drawn from these data:

(1) Films from aqueous acidic electrolytes are less dense than those from neutral or nonaqueous electrolytes.

(2) Films formed with the polymeric polystyrenesulfonate anion are more dense than those prepared under similar conditions with the sulfate anion (0.9 vs 0.5 g/cm^3, from acidic solution) or with the BF_4^- anion (1.7 vs 1.5 g/cm^3, from neutral solution).

(3) Films prepared from acetonitrile tend to be electrically more conductive than those prepared from aqueous electrolytes. This may be a consequence of shorter polymer chains in the latter materials, which contain more oxygen (see Table 2) as would be expected for frequent chain termination via carbonyl groups.

(4) Films formed with polymeric anions tend to be more conductive than those deposited with sulfate as the dopant. This suggests that the long polymer anions may help orient the polypyrrole chain growth and perhaps inhibit chain termination. A dodecylsulfate film, for example, exhibited conductivity at least as high as that of the polystyrenesulfonate material, though its mechanical integrity was poorer.

Table 1. Electrodeposition Conditions for Free-Standing Polypyrrole Films

Anion	Electrolyte	Current Density (mA/cm^2)
HSO_4^-	0.30 M pyrrole 0.23 M H_2SO_4 (pH 1.25)	3.5
PSS (acid)	0.23 M pyrrole 0.055 M polystyrenesulfonic acid (pH 1.7)	2.15
PSS (sodium)	0.34 M pyrrole 0.062 M Na polystyrenesulfonate (pH 4.2)	3.57
PAS	0.35 M pyrrole 0.022 M poly(2-acrylamido-2-methyl-1-propanesulfonic acid) (pH 2.4)	1.75
BF_4^-	0.05 M pyrrole [Ref. 18] 0.1 M Et_4NBF_4/Acetonitrile	0.50

where PSS = polystyrenesulfonate

PAS = polyacrylamidomethylpropanesulfonate

Table 2. Composition of Polypyrrole Films

Anion	Approximate Composition	Elemental Analysis Element	Calcualted	Actual
HSO_4^-	87% $C_4H_3N(HSO_4)_{0.22}$ 13% oxygen	Carbon	48.12	48.81
		Hydrogen	3.25	3.99
		Nitrogen	14.03	12.74
		Sulfur	7.07	7.01
PSS (acid)	92% $C_4H_3N(C_8H_7SO_3)_{0.25}$ 8% oxygen	Carbon	60.04	57.36
		Hydrogen	3.99	4.69
		Nitrogen	11.67	12.63
		Sulfur	6.68	7.08
PAS	91% $C_4H_3N(C_7H_{12}NSO_4)_{0.20}$ 9% oxygen	Carbon	55.67	54.74
		Hydrogen	4.67	5.52
		Nitrogen	14.43	14.28
		Sulfur	5.50	5.58

Table 3. Properties of Free-Standing Polypyrrole Films

Anion	Quantity Deposited (C/cm^2)	Measured Thickness (mil)	Density (g/cm^3)	Conductivity ($\Omega^{-1}cm^{-1}$)
HSO_4^-	39.6	8.5	.56	1.5
PSS (acid)	41.8	7.3	.88	12.5
PSS (sodium)	37.5	4.2	1.7	2.7
PAS	38.5	8.5	0.77	7.7
BF_4^- [Ref. 18]	8	0.8-1.2	1.5	10-100

These results demonstrate the excellent potential for improvement of a given film material by modification of the deposition conditions/film composition, and indicate that attention should be focused on deposition from non-aqueous solvents with large anions. The latter also do not exchange with the electrolyte anions during film reduction/oxidation, which should further inhibit degradation at the film-semiconductor interface. Polystyrenesulfonate anions have also been found to greatly increase the mechanical flexibility of polypyrrole films.

The effect of very large dopant anions in polypyrrole was investigated with films prepared on Pt with polystyrenesulfonate (molecular weight = 70,000) and with tetrasulfonated copper phthalocyanine anions (deep blue) as dopants. Attempts to reduce these films resulted in very little cathodic current and no migration of the large anions out of the films, in sharp contrast with films containing smaller dopant anions [18]. The films did become insulating, however, suggesting that the immediate surface of these materials may passivate by charge compensation from supporting electrolyte cations. Some intriguing p-type photoeffects were observed with these "reduced" materials and may be attributable to the polypyrrole itself rather than to the dye anions. These effects warrant further investigation.

Recent work by Skotheim, et al [8,19] indicates that polypyrrole films grown on bare semiconductor (Si) surfaces are more porous and less ordered than films grown on Pt-modified surfaces. In this context, we examined the application of a relatively noble metal, Pd, on n-CdSe as a base for more "ordered" polypyrrole deposition. The effect of small amounts of Pd deposited by immersing the photoelectrodes in dilute aqueous $PdCl_2$ solutions was dramatic. Figure 1 shows power curves in aqueous $Fe(CN)_6^{3-/4-}$ (pH 13) for n-CdSe with varying amounts of Pd on the surface. Three seconds in the 10^{-5} M solution reduced the V_{oc} by 160 mV relative to the bare electrode; longer exposure times cut the photoresponse drastically. These results indicate that the quantity of noble metal deposited onto the CdSe surface is critical to optimum performance of the material and that it can be controlled by chemical

means. Additionally, chemical deposition presumably takes place on active semiconductor sites, possibly the same sites upon which pyrrole polymerization would initiate. Further work in this area will involve the more noble metals, Au and Pt, upon which polypyrrole appears to deposit with the best morphology [8].

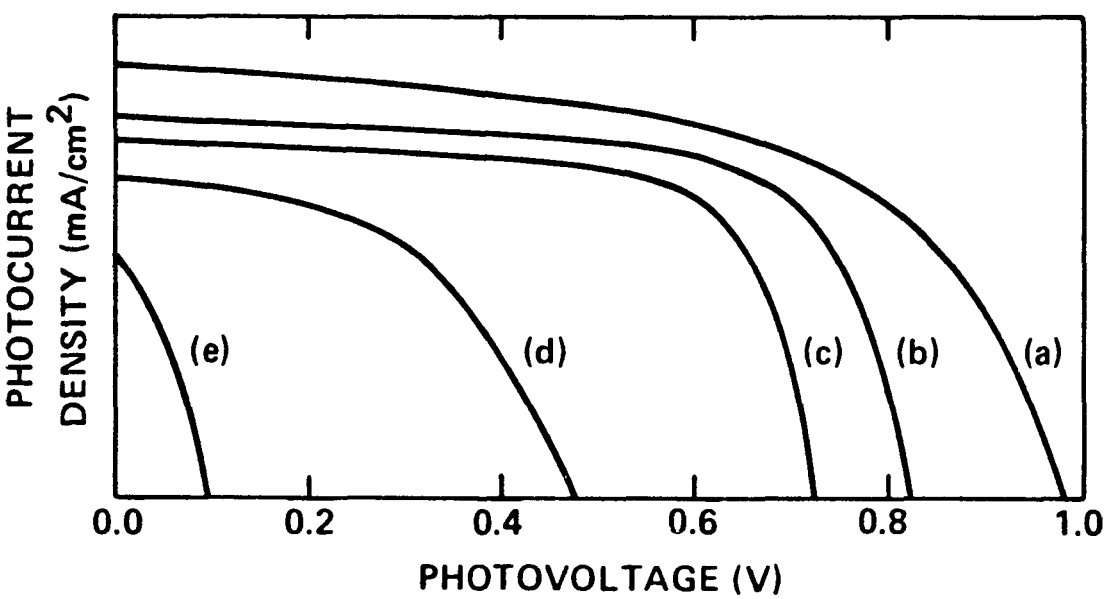

Fig. 1 Power curves in aqueous $Fe(CN)^{3-/4-}$ solution for n-CdSe with varying amounts of ^{6}Pd deposited by immersion in $PdCl_2$ solutions for various times: (a) base electrode; (b) 3 sec in 10^{-5} M; (c) 5 sec in 10^{-5} M; (d) 5 sec in 10^{-4} M; and (e) 5 sec in 10^{-3} M $PdCl_2$ solutions.

3.2 Electrochemical Photocapacitance Spectroscopy (EPS)

A paper describing the EPS method in detail has recently been prepared for publication and a preprint is given in the Appendix. Illustrative data included were derived from both the present thin-film program and an in-house effort focused on technique development (employing single crystal materials). The preliminary results for a-Si and p-Zn_3P_2 thin films were obtained

at the request of SERI; they are adequately described in the Appendix and will not be discussed here.

Most of the EPS work under the present contract was focused on CdSe thin films prepared by co-evaporation of the elements [20]. This was a co-operative effort between Rockwell and Grumman Aerospace directed toward elucidating the relationships between processing parameters and electronic states affecting the performance of CdSe thin-film electrodes in photoelectrochemical cells.

Key Grumman results can be summarized as follows. Data are variable but, in general, films prepared at low substrate temperatures (~ 100°C) yield higher photocurrents but lower open circuit voltages (~ 100 mV less) than those prepared at high substrate temperatures (~ 400°C) [21]. For low-substrate-temperature films, the open circuit voltage is increased by 50-100 mV and the fill factor is improved (with no loss in short circuit photocurrent) when the electrode is soaked in $ZnCl_2$ solution and potential cycled (under illumination) in aqueous polysulfide [22]. Based on Auger depth profile studies and impedance/polarization measurements this improvement has been attributed to a negative shift in U_{fb} (flatband potential) caused by incorporation of Zn in the CdSe film.

Interface states are known to play an important role in charge transfer processes at both single crystal and polycrystalline CdSe electrodes. For example, Fermi level pinning has been observed for n-CdSe in neutral sulfate electrolytes [23]; whereas for fast, one-electron redox species in nonaqueous electrolytes the open circuit voltage varies in a nearly ideal fashion as the redox potential is changed (over a limited range) [24]. It has been proposed [25] that Fermi level pinning can result from interface state densities as low as 10^{12} cm^{-2}. Interface state effects in the thin-film n-CdSe/aqueous polysulfide system have been investigated by Rajeshwar [26]. He reports that interface states associated with adsorbed sulfide ions mediate electron transfer and limit the open circuit voltage; no change in V_{oc} was observed when the electrolyte composition was varied so as to change the redox potential over a 250 mV range.

For n-CdSe, four donor states (onsets at 1.04, 1.21*, 1.34 and 0.2 eV below the conduction bandedge) have been detected by EPS. The 1.04 and 1.21 eV levels correspond to interface states associated with oxygen adsorption and play major roles in determining the electrical properties of CdSe devices (see Appendix). The 1.04 eV state predominates in aqueous solution and under vacuum conditions, resulting in a negative surface charge. At positive electrode potentials in acetonitrile solution, the 1.21 eV state occurs in higher concentrations, but can be electrochemically reduced to the 1.04 eV state at voltages near U_{fb}.

The 0.2 eV state in CdSe is of particular interest to the present work since it occurs in appreciable concentrations only in thin-film materials. As shown in Fig. 2, this state ionizes at more positive electrode potentials and is detected in co-evaporated films prepared at low substrate temperature (100°C) as a sharp capacitance decrease beginning at about 1.5 eV (820 nm) corresponding to a transition from the valence band to the state. As also shown in Fig. 2, the 0.2 eV state is not detected in co-evaporated films prepared at high substrate temperature (400°C). This is an important result indicating that the 0.2 eV level is responsible for the observed limitations on the attainable open circuit voltage for low-substrate-temperature material [21].

The 0.2 eV state in CdSe apparently resides at the interface, since it is not observed for electrodes transferred from aqueous KOH to acetonitrile electrolytes, as shown in Fig. 3. An interface state is also consistent with the high associated EPS capacitance change (several $\mu F/cm^2$) and its potential dependence.

Because of the importance of the aqueous polysulfide for stabilization of CdSe photoanodes in photoelectrochemical cells, appreciable effort was devoted to in situ investigation of various CdSe materials in the polysulfide

*A slightly higher apparent onset is observed for this state in specimens having a high concentration of the 1.04 eV state (see Fig. 8 in the Appendix).

electrolyte. Considerable quantitative variation in results was observed from electrode to electrode (batch to batch), which can be attributed to differences in the material itself since results for a given electrode were reproducible. In spite of the observed variation, some important general conclusions can be drawn from the data.

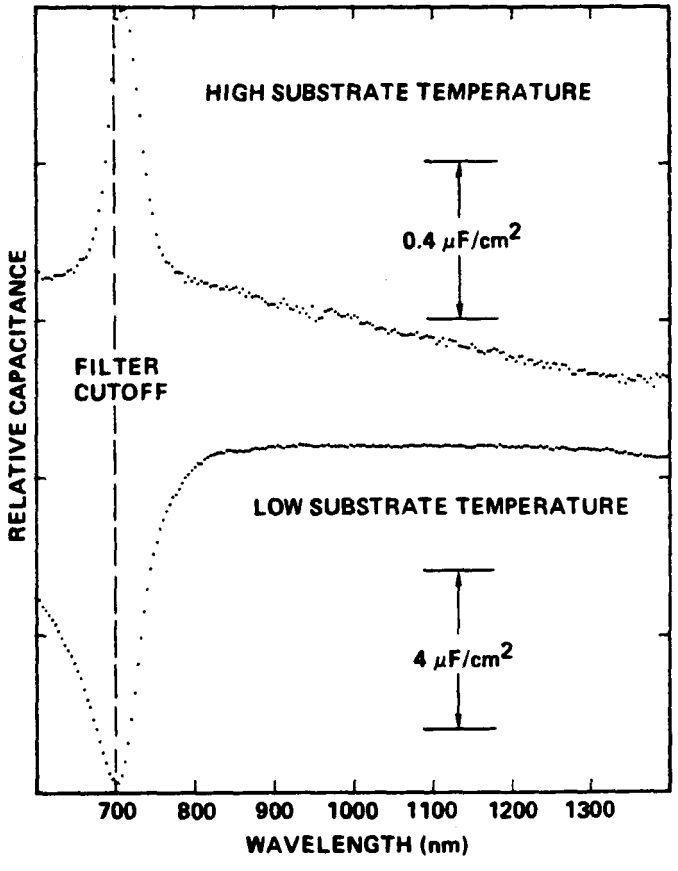

Fig 2 EPS spectra (7 Hz) measured in 0.5 M KOH at 1.0 V vs U_{fb} for co-evaporated films prepared at low (100°C) and high (400°C) substrate temperatures.

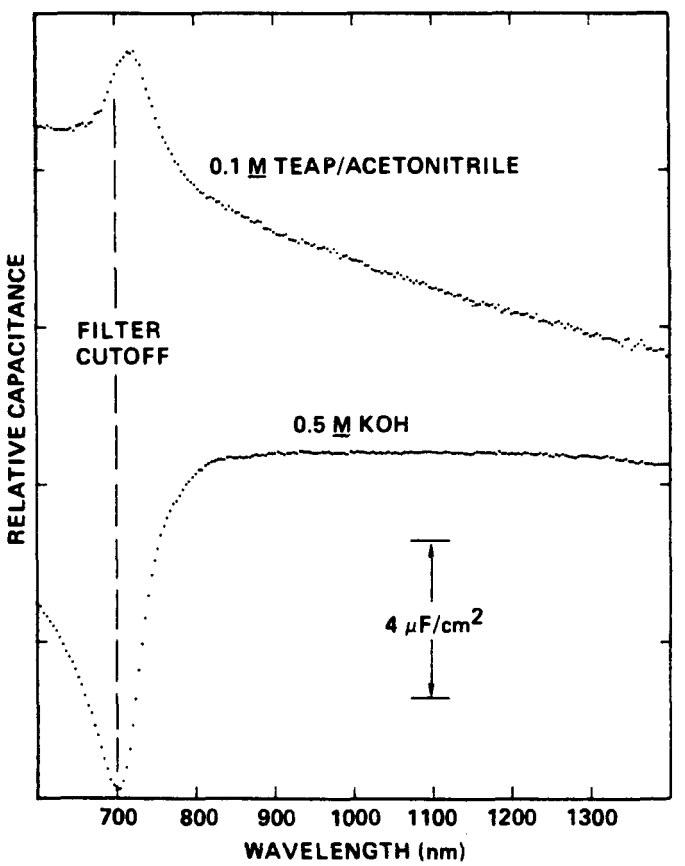

Fig. 3 EPS spectra (7 Hz) for the same low-substrate-temperature CdSe thin-film electrode at 1.0 V vs U_{fb} in 0.5 M KOH and in 0.1 M tetraethylammonium perchlorate/acetonitrile solution.

Exchange of electrons between the 0.2 eV state in CdSe and polysu - fide species in solution is dramatically evident from the time dependence of the photocapacitance under intermittent illumination, as illustrated by the curves in Fig. 4. The response time for attainment of population/depopulation

equilibrium of the state is on the order of hours in pure KOH solution, whereas in the presence of polysulfide, equilibrium is attained in less than two seconds.

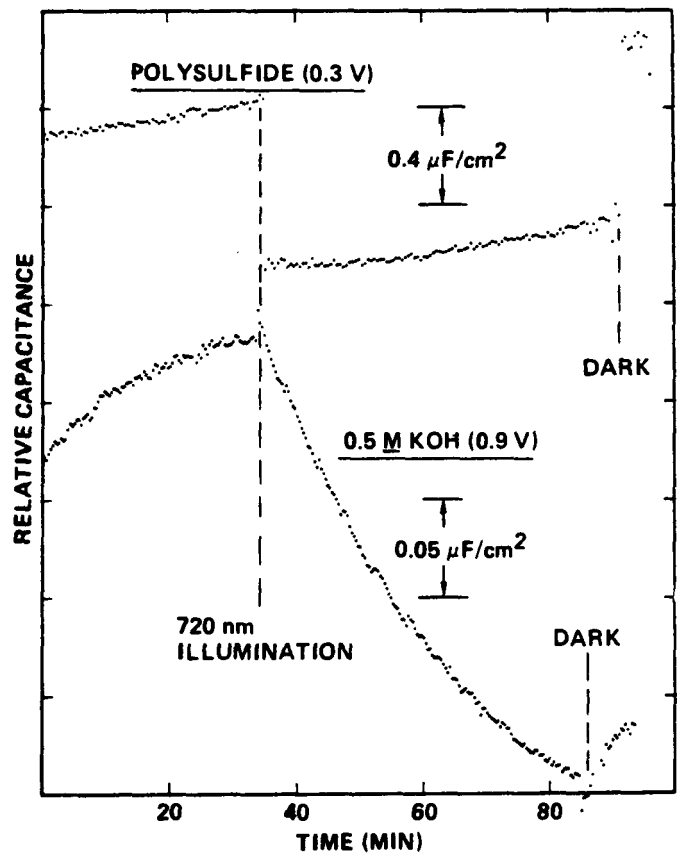

Fig. 4 Transient photocapacitance (7 Hz) for a low-substrate-temperature CdSe thin-film electrode with and without 720 nm illumination in 0.5 M KOH solution (0.9 V vs U_{fb}) and in polysulfide solution (0.3 V vs U_{fb}), i.e., 0.1 M KOH + 2.5 M Na_2S + 1.0 M S.

As evident from the EPS spectra* in Fig. 5, the population of the 0.2 eV state in the presence of polysulfide is strongly dependent on the

*Note that the perturbation frequency in this case is 70 instead of 7 Hz; frequency dispersion effects are discussed below.

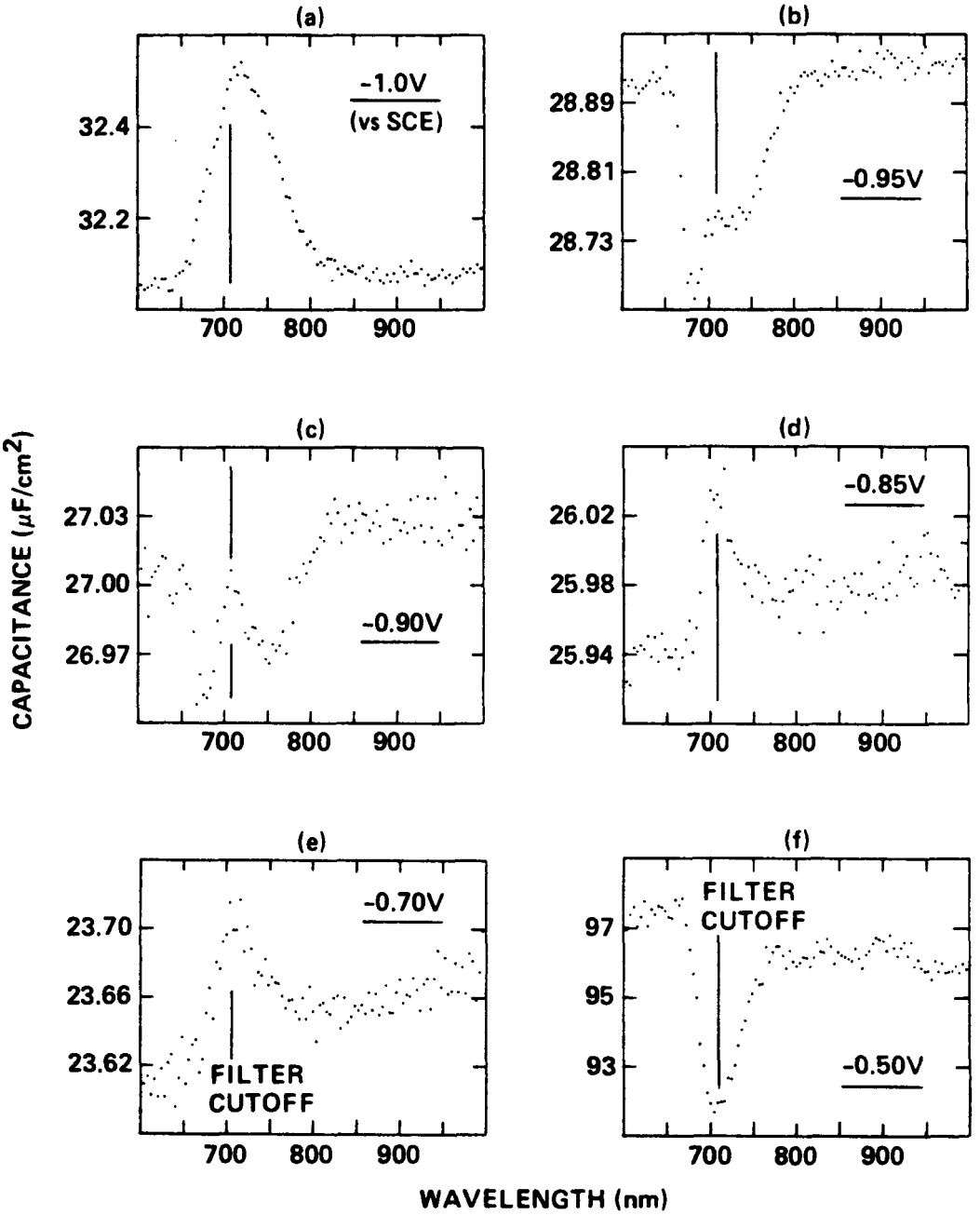

Fig. 5 EPS spectra (70 Hz) for a low-substrate-temperature n-CdSe electrode in polysulfide solution (0.1 M KOH + 2.5 M Na_2S + 1.0 M S) at various electrode potentials: (a) -1.0; (b) -0.95; (c) -0.90; (d) -0.85; (e) -0.70; and (f) -0.50 vs SCE.

electrode potential. Ionized 0.2 eV states, which are reflected in a capacitance decrease beginning at 1.5 eV (820 nm), are not observed at -1.0 V vs SCE (Fig. 5a), are evident at -0.95 and -0.90 V (Fig. 5b-c), are practically undetectable between -0.85 and -0.7 V (Fig. 5d-e), but are present in very high concentration at -0.5 V (Fig. 5f, note absolute capacitance and photocapacitance are both large). It should be emphasized that such complicated behavior is not always observed. This is not surprising since, as discussed below, the ionization/neutralization processes for the 0.2 eV state are complex and depend strongly on the density of states and U_{fb}, both of which vary appreciably from specimen to specimen.

The complex behavior illustrated in Fig. 5 can be understood in terms of interface state (surface state) reactions involving electron tunneling from the semiconductor bulk to ionized interface states (ss^+) or the reverse tunneling process from neutral interface states (ss^o), i.e.,

$$e^-_{bulk} + ss^+ \underset{(b)}{\overset{(a)}{\rightleftharpoons}} ss^o \qquad (1)$$

and reactions involving the reduced (R_{red}) and oxidized (R_{ox}) redox species, i.e.,

$$ss^+ + R_{red} \underset{(b)}{\overset{(a)}{\rightleftharpoons}} ss^o + R_{ox} \quad . \qquad (2)$$

These reactions and the relative energies (approximately to scale) of the conduction band, semiconductor Fermi level, 0.2 eV interface states and electrolyte redox level (E_R) are depicted for various bias voltages in Fig. 6. Based on photocurrent onset and ac impedance meaurements for single crystal CdSe, U_{fb} is taken as -1.5 V vs SCE, which is also consistent with the highest open circuit voltage reported for this system (0.7 V) [27] and a redox potential of -0.8 V; apparent variations from this value for polycrystalline electrodes are discussed below. It should be kept in mind that exchange of electrons between the 0.2 eV interface state and polysulfide species is conclusively evident from the much faster time constant for both ionization and neutralization of

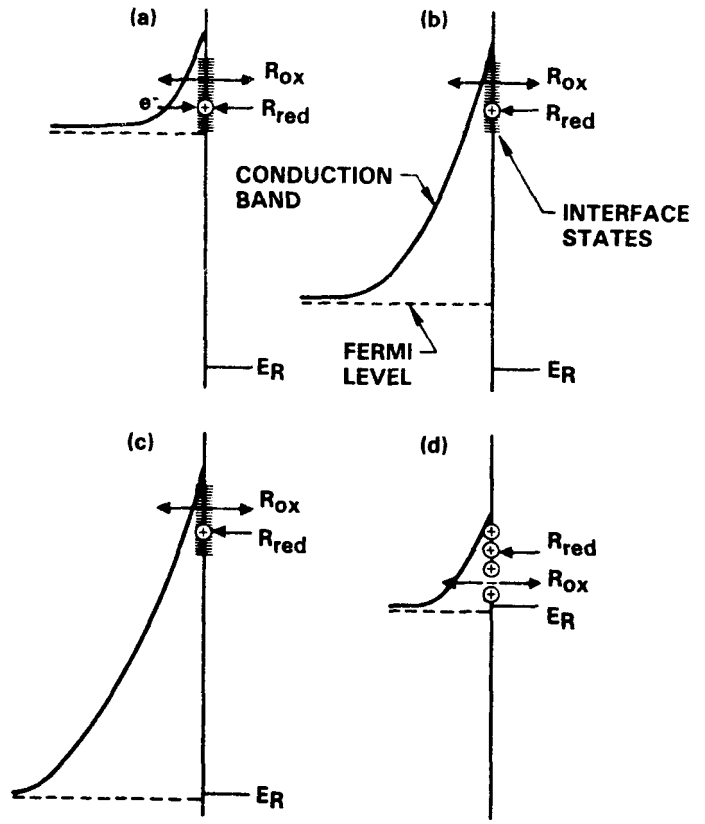

Fig. 6 Energy level diagrams for n-CdSe showing the relative positions of the conduction band, Fermi level and polysulfide redox potential for U_{fb} = -1.5 V at various electrode potentials: (a) -1.1; (b) -0.95; (c) -0.8; and (d) -0.5 V vs SCE.

the state in the polysulfide electrolyte compared to pure KOH solution (Fig. 4). For Fig. 6a-c, all of the electrode potential drop is assumed to fall within the semiconductor space charge region, which is consistent with the relatively low capacitance values.

Population of the interface states is determined by the relative rates of reactions 1a and 2a compared to 1b and 2b, which in turn are influenced by the electrode potential. In the vicinity of U_{fb} (Fig. 6a), interface states are filled by electron tunneling through the relatively thin space charge layer (Eq. 1a) and by reaction with reduced redox species (Eq. 2a); al-

though some cathodic dark current is observed, transfer of electrons to electrolyte species is relatively slow at this electrode potential so that no ionized interface states are detected (Fig. 5a). It is important to note that even when the formal E_R value lies far below the interface state energy, electron transfer from reduced redox species (filled states) is still possible, since the energy barrier is greatly reduced by the high local electric field associated with ionized interface states and by specific orbital interactions between the redox species and interface states. Because of such localized effects, E_R in the vicinity of interface states is effectively shifted negatively. At somewhat more positive potentials (Fig. 6b), electron tunneling is suppressed (Fermi level too low) so that some ionized states exist in equilibrium with electrolyte redox species (Fig. 5b-c). When the Fermi level reaches the electrolyte redox potential (Fig. 6c), net electron transfer from reduced electrolyte redox species to the semiconductor is thermodynamically favored and the ionized interface states are filled (Fig. 5d-e). As the electrode potential is made sufficiently positive of the redox potential (Fig. 6d), a large fraction of the interface states ionize by electron tunneling to the semiconductor bulk (Eq. 2b) so that a large fraction of the electrode potential drops across the electrolyte Helmholtz layer, increasing E_R relative to E_F and giving rise to an appreciable anodic dark current. In this case, the overall capacitance is large and a high density of ionized 0.2 eV interface states is detected (Fig. 5f).

The lower open circuit voltage obtained for materials containing a high concentration of the 0.2 eV interface state can readily be explained within this model. That is, at potentials closer to U_{fb} than depicted in Fig. 6a, the Fermi levl energy rises above that of the interface states, greatly increasing the probability of electron transfer to electrolyte species and, consequently, the cathodic dark current. In this case, the semiconductor bands cannot unbend further because of charge leakage to the electrolyte so that a voltage loss, corresponding to the energy of the interface states below the conduction bandedge (0.2 eV), results. This is also reflected in photocurrent onset measurements, which yield apparent U_{fb} for low-substrate-

temperature films of typically -1.3 V vs SCE rather than the -1.5 V obtained for single crystal material. Values of U_{fb} measured for such films by the ac impedance method ranged from -1.0 to -1.4 V, apparently reflecting, at least to some extent, variations in the density of ionized interface states. It should be mentioned that Reichman and Russak [21] have previously reported that Mott-Schottky plots are of questionable value in determining U_{fb} for thin-film materials of this type.

Frequency dispersion of the photocapacitance also appears to reflect the potential-dependent population/depopulation of the 0.2 eV interface state in aqueous polysulfide electrolytes. For example, in some relatively narrow potential regions, the photocapacitance decrease associated with this state was often much different in magnitude at the lower perturbation frequency (7 Hz) than at the higher frequency (70 Hz); in some cases, the 0.2 eV state was not observed at all at one of the frequencies. Such results indicate that the population of the interface state is affected by the perturbation voltage itself but only at sufficiently low frequencies for which electrons are induced to exchange between the state and electrolyte redox species or the semiconductor bulk (via tunneling). It should be mentioned that measurements of the photocapacitance frequency dispersion could ultimately yield rate constants for specific processes.

To further elucidate the role of the 0.2 eV interface state in charge transfer processes at n-CdSe electrodes, ac impedance measurements were performed over a broad frequency range (10,000 to 0.1 Hz), both in the dark and under illumination with 750 nm (1.65 eV) light. The data will be discussed in terms of the equivalent circuit given in Fig. 7, where R_S = series resistance, C_p = parallel capacitance, and R_{CT} = the charge transfer resistance. Note that C_p is a series combination of the space charge (C_{SC}) and Helmholtz layer (C_H) capacitances. In complex impedance plots of the imaginary (Z") vs real (Z') impedance components, generally R_{CT} is the diameter of the semicircle and $C_p = 1/2\pi f_m R_{CT}$, where f_m is the frequency at the maximum in the semicircle.

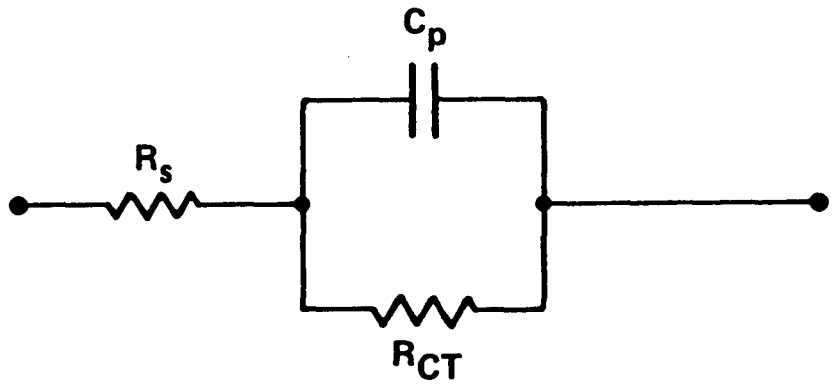

Fig. 7 Simple equivalent circuit for n-CdSe/polysulfide system.

Complex impedance plots and calculated C_p and R_{CT} values for a low-substrate-temperature n-CdSe electrode in aqueous polysulfide at three electrode potentials are shown in Fig. 8, and the corresponding EPS spectra at two perturbation frequencies (7 and 70 Hz) are given in Fig. 9. At -1.0 V, which is near U_{fb}, the semiconductor space charge capacitance is relatively large and 0.2 eV states are readily filled via electrons tunneling from the semiconductor bulk. In this case, the 1.5 eV (820 nm) transition is not observed in the EPS spectrum for either frequency and well-defined semicircles, presumably associated with double layer charging and charge transfer/adsorption processes at the interface*, are observed in the complex impedance plots. Note that the calculated double layer capacitance ($C_p = C_H = \sim 60\ \mu F/cm^2$) has not been corrected for surface roughness; if a value of 20 $\mu F/cm^2$ is assumed, the roughness factor is about 3. Although the sub-bandgap light (750 nm) has no appreciable effect on C_p, as expected when C_H is dominant, R_{CT} is decreased by almost a factor of two by such illumination. This effect is probably the result of electron-hole pair photogeneration, i.e., band tailing.

*Since no linear region is observed, diffusional processes are apparently unimportant over the frequency range studied.

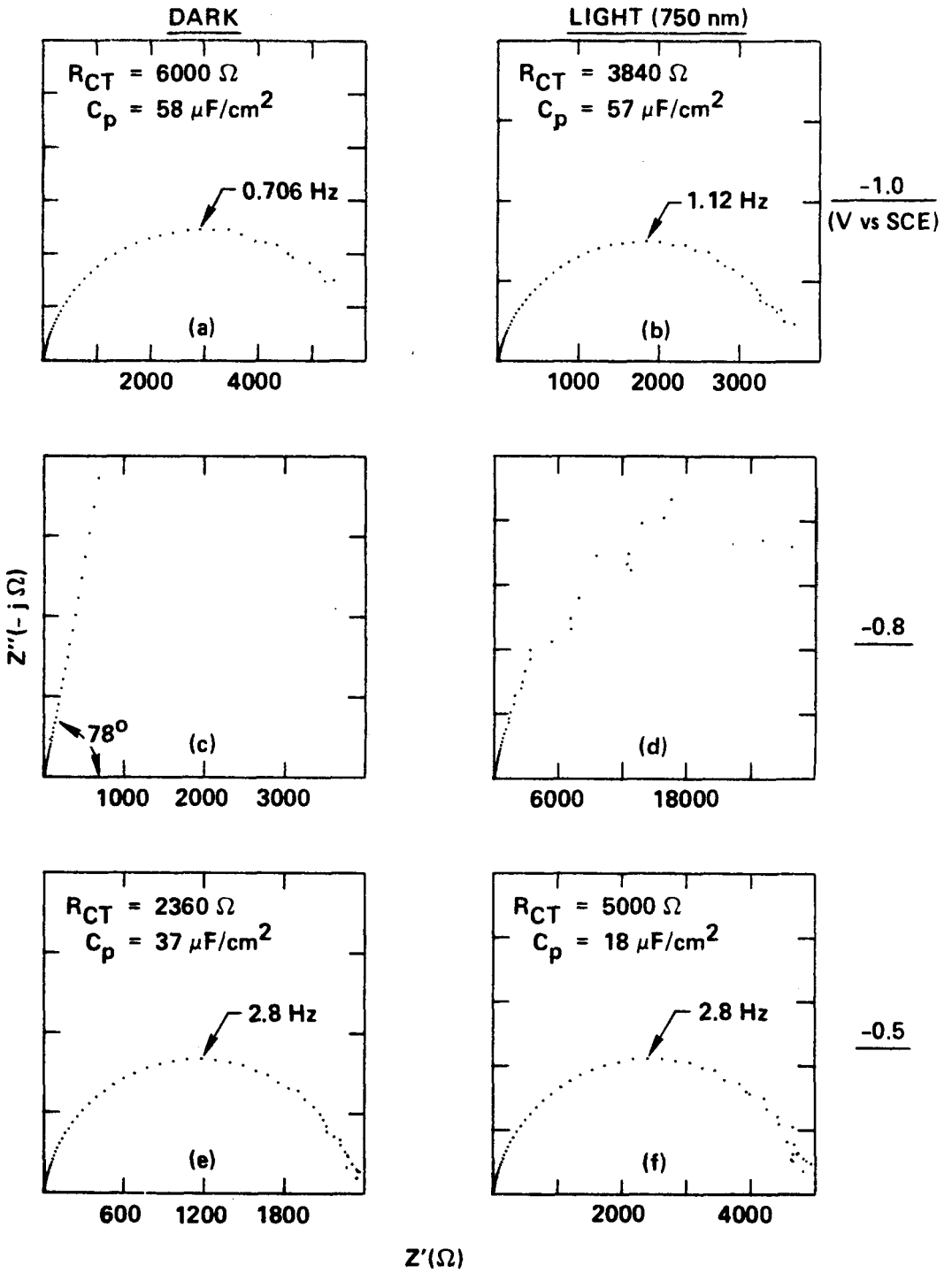

Fig. 8 Complex impedance plots for a low-substrate-temperature n-CdSe electrodes at three bias potentials in polysulfide solution (0.1 M KOH + 2.5 M Na_2S + 1.0 M S), with and without 750 nm illumination.

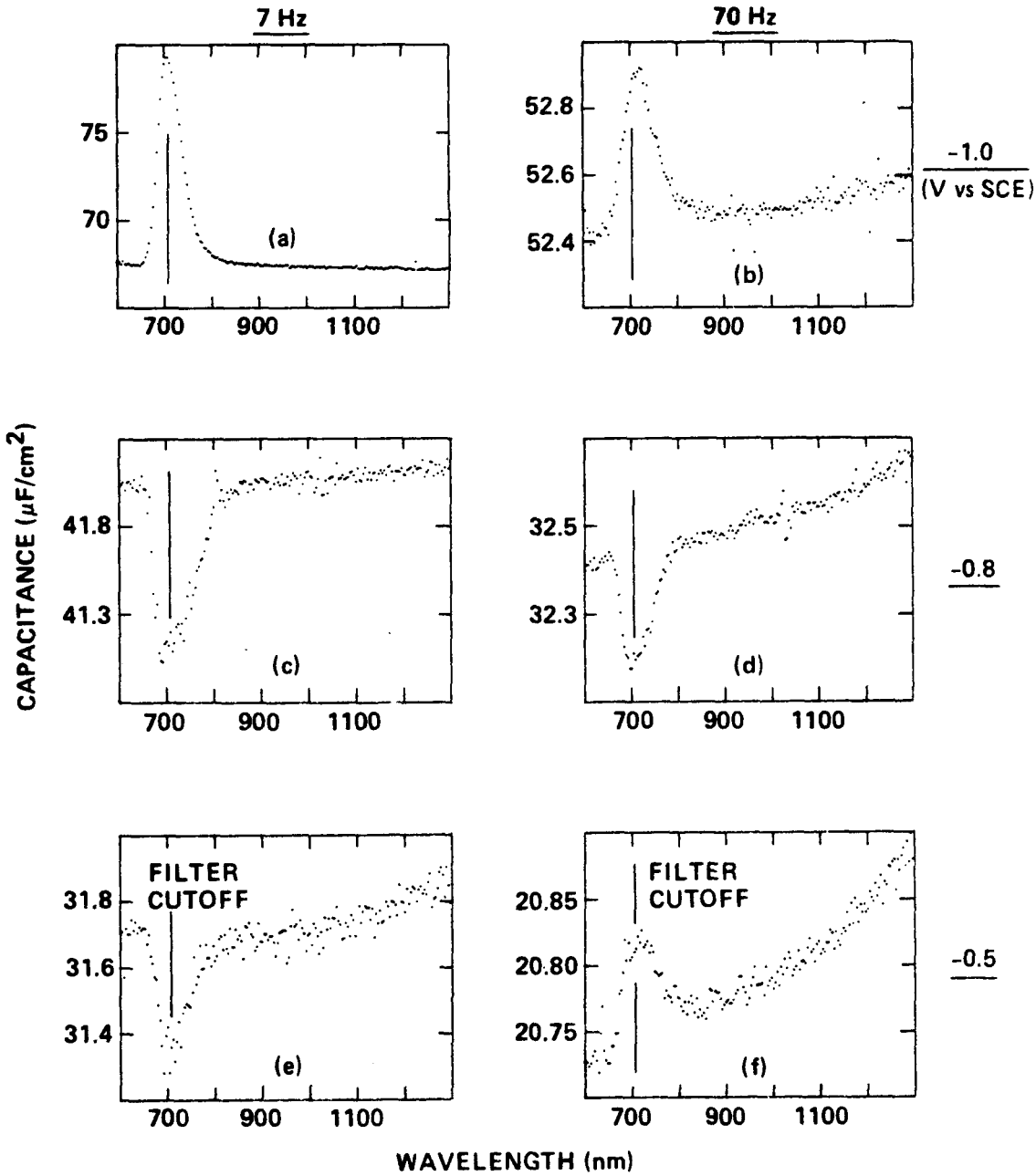

Fig. 9 EPS spectra (measured at 7 and 70 Hz) for n-CdSe at three bias potentials in polysulfide solution (same electrode and electrolyte as for Fig. 8).

At -0.8 V vs SCE, the situation is quite different. In this case, the 0.2 eV state is at least partially ionized and the 1.5 eV (820 nm) transition is observed in the EPS spectra (note that the magnitude of the capacitance decrease is smaller at the higher perturbation frequency). In the dark, the complex impedance plot is a straight line inclined at 78°, indicating that the impedance is dominated by a somewhat "leaky" capacitor (an ideal capacitor would yield an angle of 90°), presumably the space charge capacitance (C_{sc}). This is consistent with the model presented above, according to which electron tunneling from the semiconductor bulk to 0.2 eV interface states does not occur at this bias voltage so that interfacial charge transfer processes are subdued. With 750 nm illumination, the complex impedance plot exhibits significant curvature (the radius corresponding to 10^5 Ω), presumably associated with interfacial reaction of electrons photoexcited to the interface states. Since photogenerated holes are rapidly consumed at the interface, such interfacial reaction of electrons corresponds to charge carrier recombination via electrolyte species. These results, therefore, provide strong evidence for the participation of the 0.2 eV state in recombination.

At -0.5 V vs SCE, which is positive of the polysulfide redox potential, faradaic processes once again dominate the impedance, yielding a well-defined semicircle in the complex impedance plots. In this case, electrons are transferred from the reduced redox species to the interface states, then tunnel to the semiconductor bulk, resulting in an anodic dark current. The lower value of C_p compared to that at potentials near U_{fb} indicates a significant contribution from C_{sc}; under illumination, which populates and thus reduces the density of ionized interface states, the contribution is larger (C_p is smaller). Illumination also reduces R_{CT} in this case since more electrons are available for tunneling. Although the 0.2 eV state is detected in the EPS spectrum at 7 Hz (as expected), it is not observed at 70 Hz. This is probably a consequence of the relatively low density, of the 0.2 eV state for this specimen (dark capacitance is relatively low for this potential), which enhances the importance of the perturbation voltage in populating/depopulating the state.

EPS was also used to investigate the mechanism by which zinc treatment improves the performance of n-CdSe photoanodes [22]. Although this treatment (soaking in 0.1 M $ZnCl_2$ solution) apparently reduces the concentration of the 0.2 eV interface state in some cases - results of one set of experiments are summarized in Table 4 - the effect is not consistently observed and is apparently related only incidentally to the performance improvement. This interpretation is consistent with the findings of Reichman and Russak [22] that Zn, which is incorporated in the CdSe lattice, improves the open circuit voltage by shifting U_{fb} negatively.

Table 4. Effect of $ZnCl_2$ Treatment on Photocapacitance Change for 0.2 eV State in Thin-Film CdSe

Electrode Preparation	$\Delta C(\mu F/cm^2)$*
Untreated (Etched/Cycled in Polysulfide)	-0.80
30 Minute Soak in 0.1 M $ZnCl_2$	-0.70
Additional 30 Minute Soak in $ZnCl_2$ Solution	-0.60
4 Days in $ZnCl_2$ Solution	-0.47

* Measured at 7 Hz and 0.4 V vs U_{fb}.

Some speculation concerning the origin of the 0.2 eV state is in order. A chemical impurity seems unlikely since the 0.2 eV state is observed in small concentrations even for single crystal material. Also, secondary ion mass spectroscopy (SIMS) profiling of low-substrate-temperature films indicated that impurity levels are as low as those of the best high-substrate-temperature films [28], for which the 0.2 eV state is not detected by EPS. Since the concentration of the state is enhanced by mechanical polishing, participation of a lattice defect is implied. This is consistent with the findings of Brillson [29] that the feature corresponding to the 0.2 eV state in surface photovoltage spectra is enhanced by argon bombardment. Frese [23] has

inferred the presence of an interface state in CdSe centered about 0.2 eV below the conduction bandedge and attributed it to excess selenium. Although free Se would be expected to dissolve in aqueous polysulfide, a Se species bound to a lattice defect would appear to be a likely prospect as the origin of the 0.2 eV interface state. The occurrence of such a selenium-defect state would not be surprising, since as-deposited low-temperature films contain a 3:1 molar ratio of Se to Cd and are only partially crystalline. It is only after heat-treatment and removal of excess Se that such films are crystalline and exhibit favorable photovoltaic characteristics. This type of defect is also consistent with our inference that this state shifts U_{fb} anodic by interfering with polysulfide adsorption, which should be favored on Cd sites but inhibited on Se.

4.0 FUTURE DIRECTIONS

In the polymer films area, work to date indicates that deposition from nonaqueous solvents with large cations is the most promising approach to producing polypyrrole films of sufficient density and conductivity to afford photoanode protection without appreciably degrading cell performance. Attention should now be focused on the substrate-film interface and the early stages of deposition, which also exert a pronounced influence on the film properties. In addition, a viable method for improving polymer chain alignment (order) within such films would represent a major advance.

In applying EPS to the development of cadmium chalcogenide thin-film materials, emphasis should now be placed on the quantitative aspects of the method. In particular, definitive correlations between the interface state density (measured by EPS)*, cell performance parameters, and the film preparation conditions are needed. Note that progress in establishing such correlations has been hampered by film peeling problems associated with the procedure used to mount electrodes for EPS studies; these problems have been solved. Valuable insight for improving the film deposition process would also be gained if the origin of the 0.2 eV interface state could be established.

*For the 0.2 eV state whose energy lies too close to the conduction band to permit direct determination of its absolute density, curve fitting techniques must be employed (see Appendix) or relative densities must be utilized.

5.0 REFERENCES

1. R. Noufi, D. Tench, L. F. Warren, J. Electrochem. Soc. 127, 2310 (1980).

2. R. Noufi, D. Tench, L. F. Warren, ibid. 128, 2596 (1981).

3. R. Noufi, A. J. Nozik, J. White and L. F. Warren, ibid. 129, 2261 (1982).

4. R. Noufi, A. J. Frank and A. J. Nozik, J. Am. Chem. Soc. 103, 1849 (1981).

5. F. R. Fan, B. L. Wheeler, A. J. Bard and R. Noufi, J. Electrochem. Soc. 128, 2042 (1981).

6. T. Skotheim, I. Lundström, A. E. Delahoy, F. J. Kampas and P. E. Vanier, Appl. Phys. Lett. 40, 281 (1982).

7. T. Skotheim and I. Lundström, J. Electrochem. Soc. 129, 894 (1982).

8. T. Skotheim, D. Inganas, J. Prejza and I. Lundström, Mol. Cryst. Liq. Cryst. 83, 329 (1982).

9. A. J. Frank, Mol. Cryst. Liq. Cryst. 83, 341 (1982).

10. R. Haak, C. Ogden and D. Tench, J. Electrochem. Soc. 129, 891 (1982).

11. F. R. Fan, G. A. Hope and A. J. Bard, J. Electrochem. Soc. 129, 1647 (1982).

12. L. Thompson and J. DuBow, J. Electrochem. Soc. 129, 1934 (1982).

13. H. Gerisher, F. Decker and W. Kautek, Sol. Energy R&D in the Europ. Comm., Ser. D, 1, 88 (1982).

14. C. M. Gronet and N. S. Lewis, Nature 300, 733 (1982).

15. C. M. Gronet, N. S. Lewis, G. Cogan and J. Gibbons, Proc. Natl. Acad. Sci. USA (Chemistry) 80, 1152 (1983).

16. S. Menezes, B. Miller and K. J. Bachmann, J. Vac. Sci. Technol. B1, 48 (1983).

17. D. Tench and L. F. Warren, J. Electrochem. Soc. 130, 869 (1983).

18. A. F. Diaz, J. J. Castillo, J. A. Logan and W-Y Lee, J. Electroanal. Chem. 129, 115 (1981).

19. J. Prejza, I. Lundstrom and T. Skotheim, J. Electrochem. Soc. 129, 1685 (1982).

20. M. A. Russak, J. Reichman, H. Witzke, S. K. Deb and S. N. Chen, J. Electrochem. Soc. 127, 725 (1980).

21. J. Reichman and M. Russak, J. Electrochem. Soc. 128, 2025 (1981).

22. J. Reichman and M. A. Russak, J. Appl. Phys. 53, 708 (1982).

23. K. W. Frese, Jr., J. Appl. Phys. 53, 1571 (1982).

24. A. Aruchamy, J. A. Bruce, S. Tanaka and M. S. Wrighton, J. Electrochem. Soc. 130, 359 (1983).

25. A. J. Bard, A. B. Bocarsly, F. F. Fan, E. G. Walton and M. S. Wrighton, J. Am. Chem. Soc. 102, 3671 (1980).

26. K. Rajeshwar, J. Electrochem. Soc. 129, 1003 (1982).

27. B. Miller, A. Heller, M. Robbins, S. Menezes, K. C. Chang and J. Thompson, Jr., J. Electrochem. Soc. 124, 1019 (1977).

28. M. Russak, private communication.

29. L. J. Brillson, Surf. Sci. 69, 62 (1977).

6.0 APPENDIX

Preprint of a paper, entitled "Electrochemical Photocapacitance Spectroscopy Method for Characterization of Deep Levels and Interface States in Semiconductor Materials," which has been submitted for publication in the Journal of the Electrochemical Society.

ELECTROCHEMICAL PHOTOCAPACITANCE SPECTROSCOPY METHOD FOR CHARACTERIZATION OF DEEP LEVELS AND INTERFACE STATES IN SEMICONDUCTOR MATERIALS

Ron Haak and Dennis Tench
Rockwell International Science Center
Thousand Oaks, CA 91360

ABSTRACT

The recently developed electrochemical photocapacitance spectroscopy (EPS) method for characterization of deep levels in semiconductors is described. Topics discussed include the advantages of the method, experimental considerations, and the determination of state densities and kinetic parameters (associated with state population/depopulation). Both steady-state and transient capacitance changes are treated mathematically. Data for n-GaAs, p-GaAs, n-CdSe, a-Si and p-Zn_3P_2 are presented to illustrate the wide-applicability of the method and its sensitivity to both bulk and interface states, including those observed by other characterization methods.

Key Words: semiconductor traps, electrochemical detection, gallium arsenide, cadmium selenide, amorphous silicon, zinc phosphide.

INTRODUCTION

Electrochemical photocapacitance spectroscopy (EPS) has recently been shown to be a sensitive means for characterization of deep levels in semiconductor materials [1]. In the present paper, the EPS technique is described and illustrative results are presented for a variety of single crystal and polycrystalline materials. Since the intent of the authors is to encourage and facilitate use of EPS by both physicists and electrochemists, considerable detail is given in areas expected to be unfamiliar to either group of scientists. It should also be emphasized that the focus here is on covering the practical aspects of applying the method rather than on providing a comprehensive quantitative treatment.

EPS METHOD

In EPS, the capacitance of a reverse-biased semiconductor electrode is measured as a function of the wavelength of incident sub-bandgap light. The electrostatic situation and possible phototransitions for an n-type semiconductor are depicted in Fig. 1. In the dark, all of the negative charge in the electrolyte Helmholtz layer must be compensated by fixed ionized donors so that the space-charge layer extends deep into the semiconductor. At sufficiently anodic bias voltages (except at very high charge-carrier concentrations), the space-charge capacitance is generally small (~0.1 $\mu F/cm^2$) compared to the Helmholtz layer capacitance (~20 $\mu F/cm^2$). In this case, the impedance of the interfacial region is dominated by the space charge, so that additional

charge, introduced by optical population/depopulation of traps or interface states, significantly affects the thickness of the space-charge layer and is readily detected as a change in capacitance. Transitions from bandgap states (electron traps) to the conduction band introduce additional fixed positive

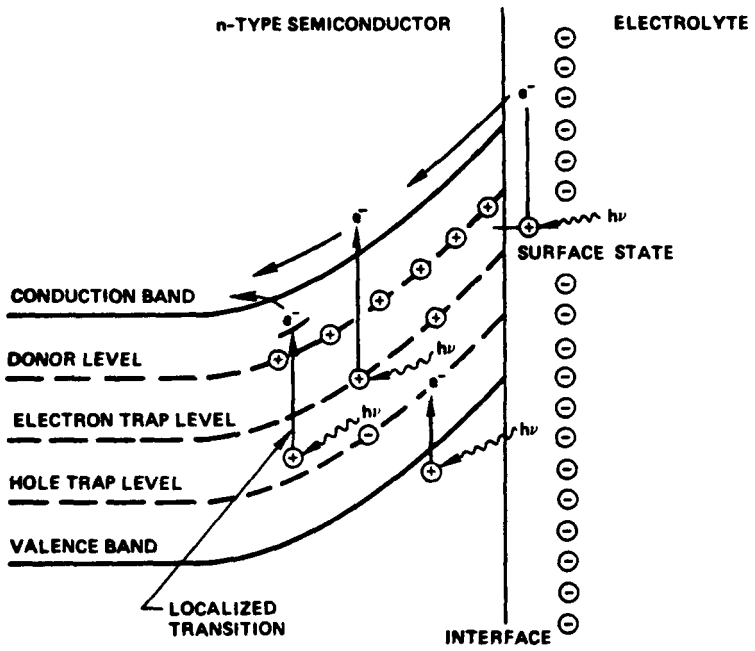

Fig. 1 Schematic representation of a reverse-biased n-type semiconductor and typical phototransitions involved in electrochemical photocapacitance spectroscopy.

charge to the semiconductor space-charge region (or at the interface), reducing the thickness of the space-charge layer and increasing the capacitance. Similarly, transitions from the valence band to bandgap states (hole traps) result in a decrease in capacitance. Charge may also be introduced into the semiconductor space charge region by localized transitions from the ground state to an excited state of an impurity (or defect center), followed by thermal injection of charge into one of the semiconductor bands (see Fig. 1). For

p-type semiconductors, the capacitance change associated with a given type of transition is opposite in sign to that for an n-type material.

Typical plots of capacitance vs wavelength (for sweeps from low to high photon energies) yield a series of plateaux and/or peaks, each corresponding to the population/depopulation of a given bandgap state. Plateaux are obtained for transitions that directly involve one of the semiconductor bands and can consequently be effected by light covering a wide range of energies above a certain threshold. Peaks are obtained for localized transitions which are effected only by light of a relatively specific energy. The onset energy of the capacitance change yields the energy of the state, relative to the appropriate bandedge. For localized transitions, the peak energy may be more descriptive. When trap saturation is attained, i.e., all states of a given energy are populated/depopulated by the available light, the magnitude of the capacitance change yields the density of states. Otherwise, the latter can often be determined from the time dependence of the photocapacitance after initiating illumination. In many cases, bulk and interface states can readily be distinguished from the effect of the electrode bias voltage, which determines the thickness of the space charge layer and thus the number of bulk states responding but has little effect on the potential drop at the interface, i.e., across the Helmholtz region.

The advantages of the EPS method can be summarized as follows. First of all, charged or discharged states produced by phototransitions generally accumulate in the space charge layer or at the interface causing an integral effect on the capacitance so that the sensitivity of EPS is greatly enhanced in comparison to techniques based on simple photocurrent measurements. Also, in

contrast to EPS, techniques based on a net flow of current cannot readily distinguish the effects of charge transfer mediators in the solution from those associated with interface states. Compared to the analogous solid-state photocapacitance technique, EPS is also more sensitive since leakage currents can be considerably reduced in electrochemical systems by adjusting the availability of electronic states in the electrolyte, and the monolayer-sharp junction with transparent electrolytes permits more light to be focused on the area of interest, i.e., the space charge region. In addition, compared to techniques like deep level transient spectroscopy (DLTS), EPS is relatively straightforward and can be performed rapidly - the blocking contact is formed simply by immersing the semiconductor in an electrolyte and measurements are performed at ambient temperature and pressure. Although slower wavelength scans requiring several hours may be required to study slow states or to minimize data scatter, EPS spectra with good resolution can often be obtained over a 2 eV range in 15 minutes. With the proper choice of electrolyte, EPS is also nondestructive. On the other hand, since EPS is an in situ electrochemical technique, the electrolyte can be chosen to permit characterization of electronic states associated with the semiconductor-electrolyte interface or passive films, e.g., oxides. EPS could also be used for electrochemical profiling, in which layers of the semiconductor are electrochemically dissolved between measurements. It should also be mentioned that EPS is sensitive to both donor and acceptor states in the same material, whereas minority carrier traps are extremely difficult to characterize by DLTS. EPS may also be applicable to the characterization of oxide films on metal electrodes.

Density of Bulk States

In calculating densities of states, it is convenient to assume that exhaustive depletion of charge carriers within the semiconductor space charge region prevails, which is justified for the small photocapacitance changes normally observed. In this case, the contribution of ionized bulk states of density n to the capacitance C is given by the well-known Mott-Schottky [2,3] expression

$$\frac{1}{C^2} = -\frac{8\pi E}{\varepsilon_{sc} e n} \tag{1}$$

for which kT/e and the potential drop in the electrolyte have been neglected (other symbols are defined below). The net number of ionized states, which determines the magnitude of the measured capacitance, is equivalent to the net semiconductor charge resulting from the equilibrium between thermal and optical emission/capture processes for both positively and negatively charged centers. Since we are concerned with the change in capacitance associated with optical population/depopulation of specific deep levels, it is appropriate to write the net density of ionized states (n_n) as

$$n_n = n_t + n_o \tag{2}$$

where n_t = density of optically populated/depopulated traps of a specific energy

n_o = net density of ionized states present under illumination with light of energy just below the onset of the transition of interest.

Note that the sign of the change in charge produced by the specific phototransition under study must be considered, i.e., n_n increases when the existing space charge is enhanced and decreases when it is diminished.

Rewriting Eq. (1) in terms of n_n and n_o and substituting in Eq. (2), we obtain

$$n_t = \pm\frac{8\pi E}{\varepsilon_{sc} e}(C_o^2 - C^2) \tag{3}$$

where C = capacitance measured with light of sufficient energy for population/depopulation of the trap

C_o = capacitance measured with light of energy just below the onset for the trap under study

E = electrode bias potential vs U_{fb} (flatband potential)

ε_{sc} = semiconductor dielectric constant

e = electronic charge.

Thus, the density of bulk traps (per cm^3) populated/depopulated by illumination can be readily calculated from the associated photocapacitance change according to

$$n_t = \pm \frac{1.4 \times 10^{20} E}{\varepsilon_{sc}} (C_o^2 - C^2) \tag{4}$$

where capacitance is in $\mu F/cm^2$ and E is in volts vs U_{fb}. When the trap is initially populated/depopulated totally and is fully depopulated/populated (saturated) by the light, $n_t = N_t$ (the total trap density). This is the case for a sufficiently deep trap (for which thermal emission is negligible) when the

associated capacitance plateau or peak is insensitive to the light intensity. An implicit assumption, of course, is that the population of only one trap level changes in the spectral region of interest.

Density of Interface States

For the treatment given here, it is assumed that interface states do not themselves respond to the measurement voltage perturbation and, therefore, affect the capacitance (only when charged) via a change in the potential distribution between the semiconductor space charge region and the electrolyte Helmholtz layer*. In this case, we rewrite the Mott-Schottky expression still assuming that the semiconductor space charge capacitance dominates the electrode impedance but now allowing for the electrode potential being distributed between the semiconductor and the electrolyte, i.e.,

$$\frac{1}{C^2} = -\frac{8\pi\Delta\phi_{sc}}{\varepsilon_{sc} e n_o} \tag{5}$$

and since

$$\Delta\phi_{sc} = E - \Delta\phi_H \tag{6}$$

and

$$\Delta\phi_H = \frac{e n_i}{C_H} \tag{7}$$

*Note that in the absence of interface states the potential drop across the Helmholtz layer is practically constant with electrode potential over the range of interest to the present work.

where $\Delta\phi_{sc}$ = potential drop across the semiconductor space charge region

n_o = bulk charge carrier concentration

$\Delta\phi_H$ = potential drop across the electrolyte Helmholtz layer

n_i = density of ionized interface states (per cm^2)

C_H = capacitance of Helmholtz layer

we have

$$\frac{1}{C^2} = -\frac{8\pi(E - \Delta\phi_H)}{\varepsilon_{sc} e n_o} = -\frac{8\pi E}{\varepsilon_{sc} e n_o} + \frac{8\pi e n_i}{\varepsilon_{sc} n_o C_H} \tag{8}$$

Since $\Delta\phi_{sc} \cong E$ when $n_i = 0$

$$\frac{1}{C^2} = \frac{1}{C_o^2} - \frac{8\pi n_i}{\varepsilon_{sc} n_o C_H} \tag{9}$$

so that

$$n_i = \pm \frac{\varepsilon_{sc} n_o C_H}{8\pi} \left(\frac{1}{C_o^2} - \frac{1}{C^2}\right) \tag{10}$$

where C = capacitance with interface states ionized

C_o = capacitance in the absence of interface state ionization.

Taking $C_H = 20\ \mu F/cm^2$, which is its typical value [4], we have

$$n_i = 8.7 \times 10^{-7}\ \varepsilon_{sc} n_o \left(\frac{1}{C_o^2} - \frac{1}{C^2}\right) \tag{11}$$

where capacitance is in $\mu F/cm^2$.

Deep Level Kinetic Characteristics

The kinetics of processes involved in filling and emptying deep trap levels can also be studied by EPS. In this case, the photocapacitance transients are measured after initiation and after interruption of illumination. The general expression* for the change in the concentration of ionized states with time is

$$\frac{dn_s}{dt} = k_i(N_s - n_s) - k_n n_s \tag{12}$$

where n_s = density of ionized states

N_s = total density of trap states

k_i = ionization constant

k_n = neutralization constant

t = time.

Note that k_i and k_n include terms for both thermal and optical processes.

Integration of Eq. (12) yields

$$\ln [(k_i + k_n)n_s - k_i N_s] = -(k_i + k_n)t + K \tag{13}$$

where K = integration constant.

*The treatment given here is similar to that presented by Miller, Lange and Kimmerling [5] except that the equations are derived in terms of ionized states.

The components of k_i and k_n depend on the nature of the state. For a state that becomes more positive when ionized

$$k_i = e_n^t + e_n^o + c_p \tag{14}$$

$$k_n = e_p^t + e_p^o + c_n \tag{15}$$

whereas for a state that becomes more negative when ionized

$$k_i = e_p^t + e_p^o + c_n \tag{16}$$

$$k_n = e_n^t + e_n^o + c_p \tag{17}$$

where e_n^t and e_p^t = thermal emission rate constants

e_n^o and e_p^o = optical emission rate constants

c_n and c_p = capture rates

for electrons and holes, respectively. The various processes involved can be visualized with the aid of Fig. 2. Note that an increase in positive charge produces an increase in C for an n-type semiconductor but a decrease for a p-type material, and a decrease in positive charge produces the opposite effects.

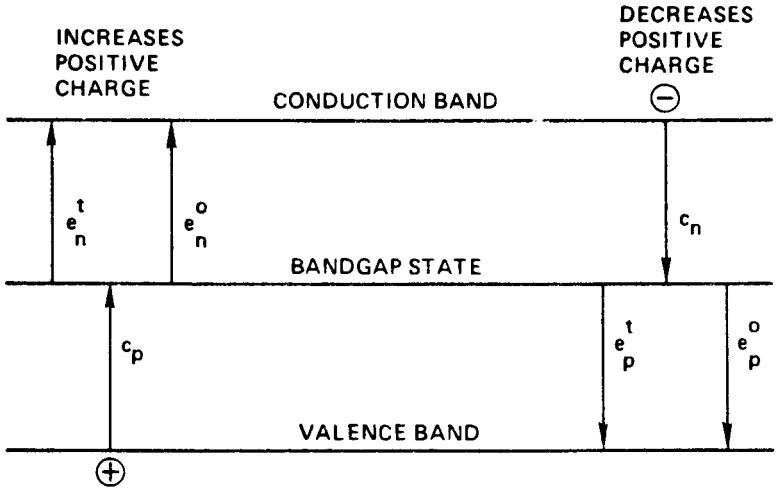

Fig. 2 Schematic diagram depicting the various ionization and neutralization processes for a semiconductor bandgap state.

The capture rates include a factor for the appropriate minority carrier concentration, i.e.,

$$c_n = \sigma_n \nu_n n \tag{18}$$

and

$$c_p = \sigma_p \nu_p p \tag{19}$$

where σ_n and σ_p = capture cross sections

ν_n and ν_p = average thermal velocities

n and p = charge carrier concentrations

for electrons and holes, respectively.

Deep Levels in Wide-Bandgap Materials

Of special interest from a practical standpoint is the characterization of deep traps in relatively wide-bandgap extrinsic semiconductors, for which thermal emission processes and the concentration of minority carriers can often be ignored. For a specific example, consider an n-type material containing a deep electron trap that is neutral when filled and positively charged when empty. In this case, e_n^t and c_p are taken as zero, i.e.,

$$k_i = e_n^o \tag{20}$$

and

$$k_n = e_p^t + e_p^o + c_n \tag{21}$$

First consider repopulation of the states in the dark after at least a portion of them have been ionized by illumination. Since e_n^o and e_p^o are also zero in this case, $k_i = 0$ and $k_n = e_p^t + c_n$ so that Eq. (13) reduces to

$$- \ln n_s = (e_p^t + c_n)t + K \tag{22}$$

Substitution of n_t and n_i from Eqs. (3) and (10) for n_s yields

$$- \ln \left[\frac{8\pi E}{\varepsilon_{sc} e} (C_o^2 - C^2)\right] = (e_p^t + c_n)t + K \tag{23}$$

for bulk states, and

$$- \ln \left[\frac{\varepsilon_{sc} n_o C_H}{8\pi} \left(\frac{1}{C_o^2} - \frac{1}{C^2}\right)\right] = (e_p^t + c_n)t + K \tag{24}$$

for interface states. Solving for K at $t = 0$, we have

$$\ln \left(\frac{C_o^2 - C_t^2}{C_o^2 - C_{t=o}^2}\right) = -(e_p^t + c_n)t \qquad (25)$$

for bulk states, and

$$\ln \left[\left(\frac{1}{C_o^2} - \frac{1}{C^2}\right)/\left(\frac{1}{C_t^2} - \frac{1}{C_{t=0}^2}\right)\right] = -(e_p^t + c_n)t \qquad (26)$$

for interface states (where C_t and $C_{t=0}$ represent C at time t and t = 0, respectively).

Thus, plots of $\ln [(C_o^2 - C_t^2)/(C_o^2 - C_{t=o}^2)]$ for bulk states or $\ln [(1/C_o^2 - 1/C_t^2)/(1/C_o^2 - 1/C_{t=o}^2)]$ for interface states vs time should yield a straight line of slope $(e_p^t + c_n)$. For states sufficiently above the valence band in energy, e_p^t can also be taken as zero and c_n is obtained directly. When this is not the case, c_n, which is proportional to n, can be evaluated from the effect of injecting a known concentration of majority carriers (electrons). This can be accomplished by momentarily reducing the bias voltage [6]. Alternatively, in electrochemical systems, it is possible to adjust the dark current, which determines the overall value of n through the space charge region, by adding appropriate solution redox couples that inject majority carriers into the semiconductor. The more negative the redox potential of the couple the greater the tendency to inject electrons. It should be mentioned that analogous procedures could be used to evaluate minority carrier capture rates from EPS measurements. In this case, minority carriers would be injected by momentarily forward biasing the semiconductor [6] or employing solution redox couples that are sufficiently positive for n-type semicondutors or sufficiently negative for p-type materials.

Now consider the change in photocapacitance with time after initiating illumination. Since $n_s = 0$ at $t = 0$, Eq. (13) becomes

$$-\frac{1}{(k_i + k_n)} \ln \left[1 - \frac{(k_i + k_n)}{k_i N_s} n_s\right] = t \qquad (27)$$

Having determined k_n from photocapacitance decay studies, we can readily calculate k_i when N_s is known, i.e., when trap saturation can be attained. Otherwise, k_i and N_s can be determined by iteration to attain the best fit for Eq. (27). If the photon flux (I) is known, the optical cross section (σ_n^o) can be extracted from e_n^o (which equals k_i in this case) since $e_n^o = \sigma_n^o I$.

EXPERIMENTAL CONSIDERATIONS

Electrolyte Selection

For studies of a specific electrochemical system, EPS measurements are, of course, made *in situ* in the electrolyte of interest. In other cases, however, an electrolyte must be selected.

Interface states associated with oxygen adsorption or surface oxides can readily be studied by EPS in aqueous solutions, in which oxide interfacial structures are apparently stable. Note that for n-CdSe (see results section), interface states associated with oxygen adsorption are found to be practically unchanged in aqueous systems compared to the vacuum. In EPS, the environment, i.e., electrode potential and solute/solvent, can also be easily varied. Such studies can provide valuable information about oxidation/passivation phenomena.

In cases for which there is flexibility in the choice of electrolyte for EPS measurements, two prime considerations are the electrolyte optical transmission and electrical conductivity. Ideally, the electrolyte should be transparent to light ranging in energy from the bandgap down to midgap, which permits the entire bandgap region to be probed (via transitions involving both bands). Solvents that are sufficiently polar can generally be rendered electrically conductive via dissolution of appropriate salts. Tetraalkylammonium salts are typically used with the nonaqueous solvents.

Optical transmission spectra for some key solvents are shown in Figs. 3 and 4; the cell path length was 1.0 mm, which is approximately equivalent to the thickness of electrolyte through which light passes in the EPS cell used in the

present work. The useful range for water (Fig. 3), which is limited by the onset of absorption associated with O-H stretching, is seen to extend down to about 0.9 eV (1350 nm). Note that the transmission cutoff for alcohols would be similar to that of water. Acetonitrile (Fig. 3) exhibits no significant

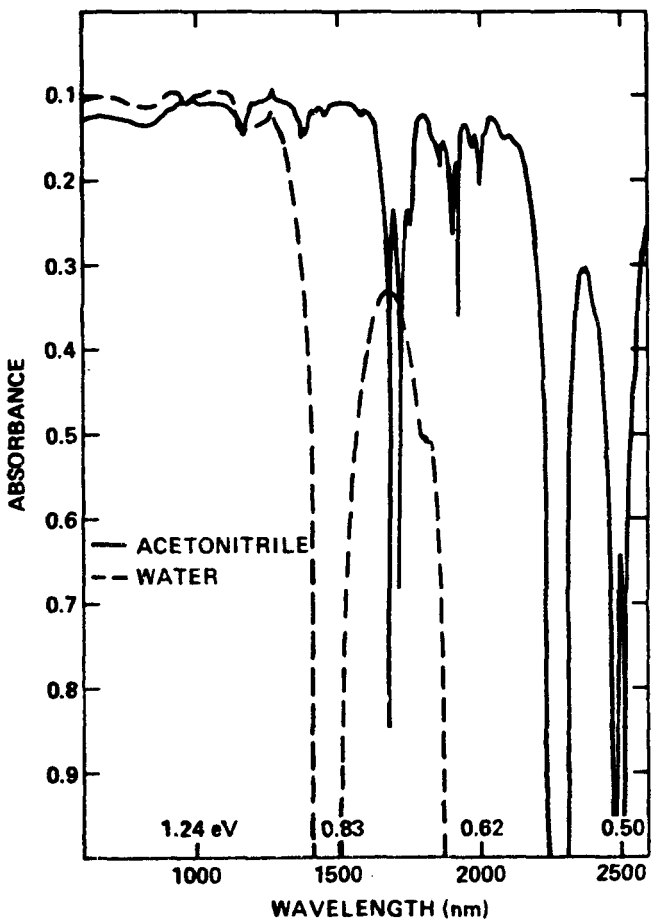

Fig. 3 Optical absorption spectra for water and acetonitrile (1.0 mm path length).

absorption features down to about 0.75 eV (1650 nm), where the onset of sharp absorption peaks associated with the C-H bond is observed. At energies between 0.75 and 0.55 eV, several sharp spectral features are evident but considerable light transmission also occurs. Thus, acetonitrile can be used with little concern down to 0.75 eV, and between 0.75 and 0.55 eV with caution. In all cases, EPS spectra should be closely examined to determine which features might be due to solvent absorption. The effects of the latter can be checked by varying the solvent or the thickness of the electrolyte layer in the light path. Chloroform, which contains only one C-H bond, exhibits significantly weaker absorption (the only pronounced spectral features are two sharp peaks, at 0.52 and 0.73 eV) so that its useful range extends to at least 0.5 eV (Fig. 4). The effects of solvent absorption features associated with hydrogen can be even further reduced by use of deuterated solvents. Figure 4 also shows the transmission spectra for deuterated chloroform (a readily available solvent); the good transmission characteristics extend to beyond 0.5 eV (the only pronounced spectral feature is a sharp peak at 0.55 eV), permitting bandgaps in the 1 eV range to be probed.

Another consideration in selecting a solvent is the stability of the semiconductor in the electrolyte. Although chemical instability may be a problem in some cases, the primary concern is the effect of photogenerated minority carriers, which migrate to the interface and can result in dissolution of the semiconductor and/or film formation. It should be emphasized at the outset that, in our experience, such effects are generally small and do not appreciably affect short-term EPS measurements. In the case of bulk states,

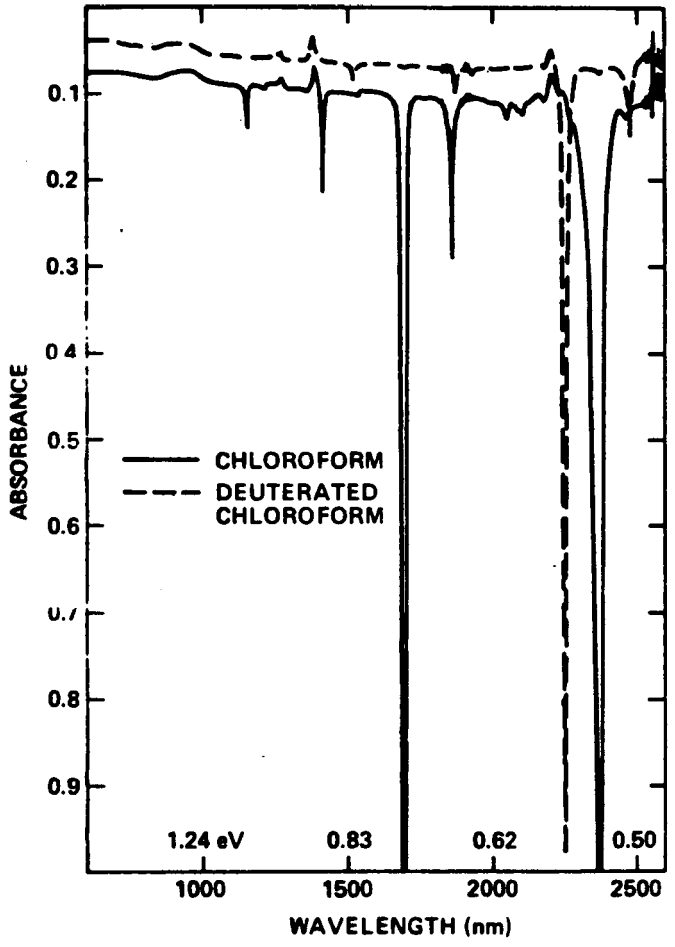

Fig. 4 Optical absorption spectra for chloroform and deuterated chlorform (1.0 mm path length).

even long-term measurements may not be affected by a slow rate of photodissolution, but film formation, when it occurs, is likely to cause the baseline capacitance to drift with time, making quantitative inferences more difficult. For studies of interface states, both photodissolution and film formation are likely to affect the structure of the interfacial region and interfere with EPS measurements. It should be mentioned that although the less polar nonaqueous

solvents generally provide greater inherent stability against semiconductor photodissolution, there is also a greater tendency toward film formation in such media.

Photodissolution and film formation processes can generally be greatly suppressed or practically eliminated by incorporation of suitable redox species in the electrolyte. In this case, photogenerated minority carriers are removed as they arrive at the interface (before semiconductor degradation can occur) by reaction with the redox species, which is simultaneously converted to another soluble species. The stabilizing effect of redox species is to some extent reflected in the redox couple potential but other factors are also important in this respect and the effect of the couple on the interface characteristics and dark current must be considered. For example, specific adsorption of redox species can affect the interfacial structure and the semiconductor/electrolyte potential distribution, and may result in an increase in dark current. Ideally, both halves of the couple should be transparent to light in the energy range of interest (or be present in small concentration) and should not adsorb strongly on the semiconductor. Fortunately, a large number of redox couples have been studied for use in stabilizing electrochemical solar cells; even the least stabilizing of those reported in the literature would probably be effective for the extremely small currents flowing during EPS measurements.

It should also be mentioned that some electrolyte redox species may exchange electrons with interface states, affecting their population and, thus, the magnitude of any corresponding EPS spectral feature. Such effects may be undesirable in some cases, but can also be exploited to investigate the extent

to which a particular interface state mediates electron transfer between the semiconductor and the electrolyte. Charge transfer mediation undoubtedly plays an important role in the functioning of many electrochemical systems, particularly those involving electrocatalysis, but its fundamental aspects have remained obscure.

Measurement Frequency

The voltage perturbation frequency employed in EPS measurements can to some extent be used as an adjustable parameter to maximize the signal to noise ratio and, thus, the sensitivity to capacitance changes. In this case, the frequency is chosen to yield a relatively large value for the capacitive reactance, as indicated by a large phase shift (70-90°) between the voltage perturbation and the current response. When there is appreciable frequency dispersion, this procedure will lead to some uncertainty in the calculated densities of states but the associated error is generally very small for smooth single crystal electrodes and is typically much less than an order of magnitude even for polycrystalline materials. In any case, measurements made at a given frequency should provide a relative measure of the density of a particular state.

Errors associated with frequency dispersion can be minimized if the source of the dispersion is known. Generally speaking, high frequency measurements, for which the effects of surface inhomogeneities and lattice defects are minimal, are considered to be more reliable. This is often not the case for polycrystalline films having appreciable porosity since, because of the tortuous

current paths involved, a large portion of the perturbation voltage at high frequencies may fall across the electrolyte rather than the semiconductor. Thus, for porous films, low frequency measurements may be more reliable.

Measurements at various perturbation frequencies can also provide additional information. For example, the exchange of electrons between interface states and electrolyte species in response to the voltage perturbation, which may occur under some bias potential conditions, is likely to be a relatively slow process that contributes to the measured capacitance only at low frequencies. In this case, the associated EPS spectral feature will vanish as the perturbation frequency is increased.

Electrode Bias Voltage

The electrode bias potential is typically varied over the range where the semiconductor is reverse-biased and the dark current is minimal. As already mentioned, the magnitude of EPS spectral features associated with bulk states generally varies linearly with the space charge depletion width, whereas those associated with interface states are relatively potential insensitive. Thus, bulk and interface states can typically be distinguished from the effect of the electrode bias potential. Identification made in this way can readily be verified by changing the solvent or adding surfactants to the electrolyte, which typically have a large effect on the energies/population of interface states but have little effect on the EPS characteristics of bulk states.

Changes in the population of interface states with electrode bias voltage can also be detected by EPS. In this case, the magnitude of the photocapacitance change corresponding to the interface state should vary rather abruptly over a limited potential range as the state population changes; this contrasts with the Mott-Schottky behavior associated with a bulk state. It should also be mentioned that the potential dependence of the population of an interface state is likely to be affected by the presence of redox species in the electrolyte, which can exchange charge with the state.

EXPERIMENTAL DETAILS

Figure 5 shows a block diagram of the apparatus used in the present work. Complete computer control is provided by a Hewlett-Packard 9826 desktop computer. The real and imaginary components of the electrode impedance are determined by a Solartron Model 1172 frequency response analyzer which automatically averages over many perturbation cycles. The perturbation voltage is typically 10 mV (rms), although larger voltages are sometimes used for highly-resistive materials. The impedance of the counter electrode (Pt) and lead inductance effects are eliminated from the measurement by use of a Stonehart Model BC 1200 potentiostat (which employs a dual working electrode lead) in the three-electrode mode. A Tektronix Model AM501 differential amplifier is employed between the potentiostat and the frequency response analyzer. Monochromatic illumination (1-2 mW/cm^2) having a bandwidth of ~8 nm (depending on the slit dimensions and diffraction grating) is provided by a 1000 W tungsten-halogen lamp* via an Instruments SA Model HT-20 turret monochromator. Appropriate ordering/neutral density filters are inserted automatically.

With the apparatus described here, capacitance changes of 0.1% can be measured. This corresponds to a detectability limit for both bulk and interface states (the latter expressed per cm^2) of 0.2% of the overall charge carrier concentration.

*The spectral output for this lamp is relatively monotonic; for most other light sources, particularly xenon lamps, it is important to take into account intensity variations with wavelength.

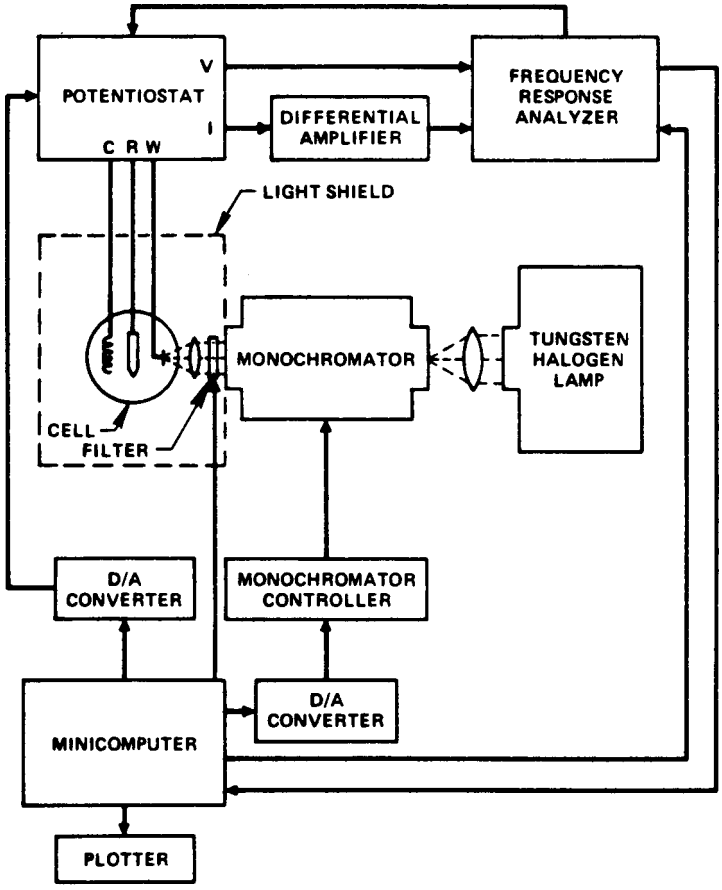

Fig. 5 Block diagram of the EPS apparatus.

The electrochemical cell was glass with a quartz optical window and a Teflon top, through which cell connections were made. The electrolyte volume was ~ 200 mL. An inert atmosphere was maintained via argon bubbling through the solution. The platinum counter electrode was isolated from the main cell compartment via a glass frit. The reference electrode was a double junction saturated calomel electrode (SCE) or Ag/AgCl in aqueous solutions, and a Ag/Ag^+ (acetonitrile/0.1 M $AgNO_3$/0.1 M tetraethylammonium perchlorate) in nonaqueous electrolytes. All bias voltages are given relative to the flat band potential (U_{fb}), which was determined by ac impedance measurements as a function of potential (values typically agreed with those observed for photocurrent onset).

Semiconductor electrodes, with appropriate ohmic contacts, were mounted in polyester resin (Torr Seal, Varian, Inc.) so that only the desired surface was exposed to the electrolyte. The area of the exposed semiconductor surface was usually 0.2 cm^2, permitting total illumination of the surface. For larger electrodes, the dark capacitance associated with the unilluminated portion of the exposed surface was subtracted from all measured capacitance values. Single crystal electrodes were generally polished using aqueous slurries of successively finer alumina powders to a particle size of 0.3 μm before etching, whereas thin-film materials received no mechanical pretreatment. The following etching procedures were used. GaAs electrodes were immersed in 50/50 v/o $H_2SO_4/H_2O_2(30\%)$ for ~10 s. CdSe electrodes were etched in ~50 v/o HNO_3 for ~10 s, then dipped in aqueous polysulfide solution (1.0 M S + 2.5 M Na_2S + 1.0 M KOH) to remove excess Se from the surface. Amorphous Si specimens were used as-obtained. Zn_3P_2 electrodes were etched in 1 v/o bromine/methanol for 5-10 s.

RESULTS AND DISCUSSION

Deep Traps in n-GaAs

The sensitivity of EPS to some of the more common deep traps in n-GaAs is illustrated by the spectrum for horizontal Bridgman material (<100>) shown in Fig. 6; corresponding phototransitions are depicted in the insert. The important features apparently correspond to the "B" state [7,8] (decrease in

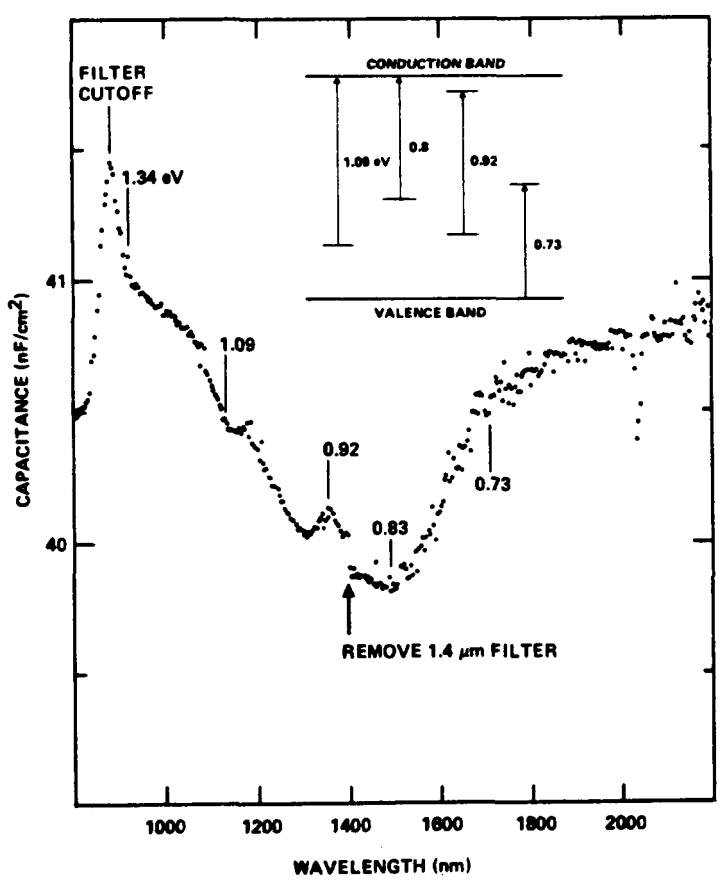

Fig. 6 EPS spectrum (measured at 5 kHz) and associated energy levels/phototransitions for n-GaAs (0.5 V vs U_{fb}) in 0.1 M tetraethylammonium perchlorate/acetonitrile solution.

capacitance at 0.73 eV), the "EL2" level [9,10] (increase in C at 0.83 eV), chromium [11] (peak at 0.92 eV superimposed on EL2 wave), and an unidentified donor state at 1.09 eV. All of these transitions exhibit the electrode potential dependence expected for bulk states. On the other hand, some surface pretreatments introduce an additional donor state at about 0.70 eV which apparently resides at the interface, since the associated capacitance change is potential independent. Based on the capacitance changes, the densities of all bulk states detected are $\sim 10^{14}/cm^3$, which are reasonable values when compared to literature data for similar material. Also, SIMS (secondary ion mass spectroscopy) analysis indicated that the chromium concentration in our material was $2 \times 10^{14}/cm^3$.

Comparison with DLTS

A direct comparison between EPS and DLTS has been made for an LEC (liquid encapsulated Czochralski) p-GaAs specimen (<100>); a typical EPS spectrum and the assumed phototransitions are shown in Fig. 7. With DLTS, only one state was detected - the hole trap (acceptor level) corresponding to the sharp capacitance increase at 0.69 eV in the EPS spectrum. Both methods yielded about the same density for this state, i.e., $10^{15}/cm^3$. Three additional states were detected by EPS, corresponding to a capacitance decrease at $\sim$ 0.74 eV (electron trap), a peak at 0.9 eV (probably a localized impurity transition), and an increase in capacitance at 1.06 eV (hole trap). Although the sum of the energies of the 0.69 and 0.74 eV levels corresponds closely to the bandgap (1.42 eV), complementary transitions involving the same center are not involved. This was shown clearly from the time dependence of the capacitance

upon shifting the wavelength from one value to another or interrupting illumination. For example, if 1500 nm light is blocked, the capacitance rapidly increases to a slowly decaying value since the lifetime of the occupied 0.74 eV level is relatively short (< 1 s), whereas that of the occupied 0.69 eV hole trap is very long (at least several minutes).

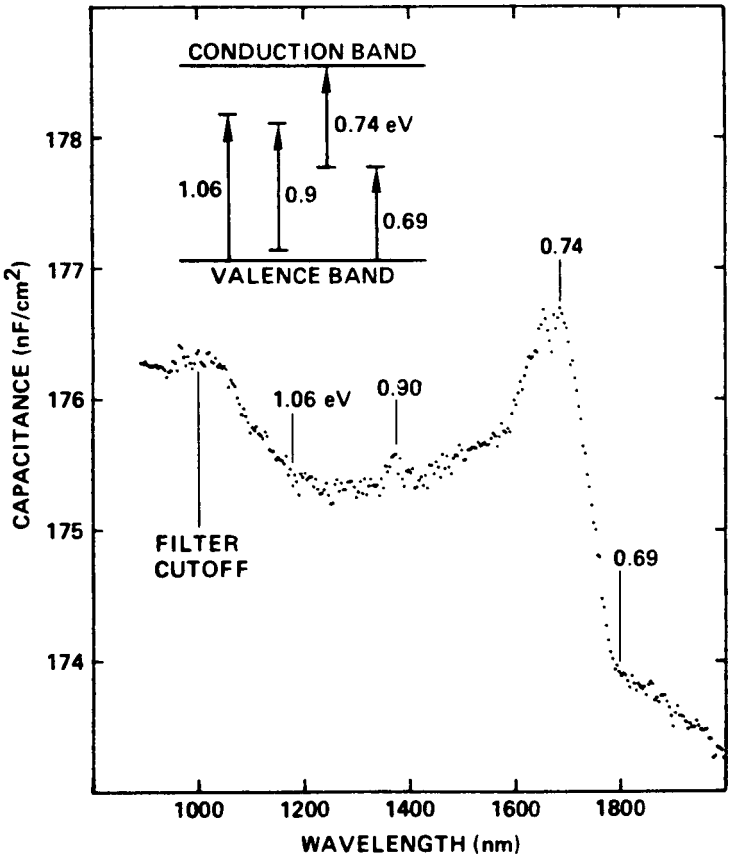

Fig. 7 EPS spectrum (measured at 10 kHz) and associated energy levels/phototransitions for LEC p-GaAs (0.4 V vs U_{fb}) in 0.1 M tetrabutylammonium perchlorate/0.1 M benzoquinone/acetonitrile.

Interface States at n-CdSe

The sensitivity of EPS to interface states is best illustrated by data obtained for n-CdSe, for which interface states associated with oxygen adsorption play a dominant role [12,13]. Figure 8 shows an EPS spectrum and associated phototransitions for a chemically-etched single crystal of n-CdSe

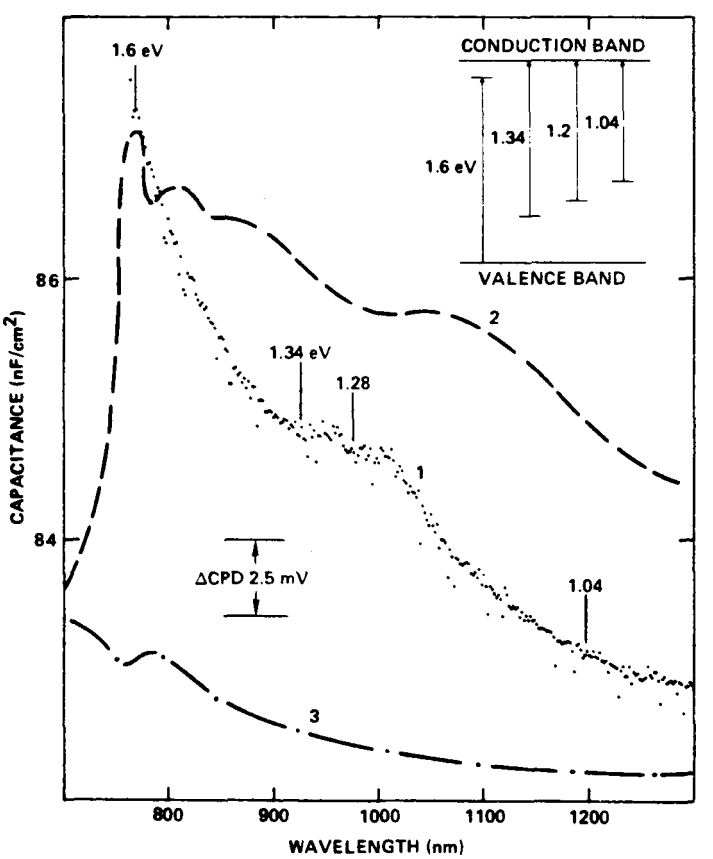

Fig. 8 EPS spectrum (measured at 5 kHz) for chemically-etched single crystal n-CdSe (0.7 V vs U_{fb}) in 0.5 M KOH solution (curve 1) and surface photovoltage spectra for oxygen-adsorbed (curve 2) and vacuum-cleaved (curve 3) single crystal n-CdSe (surface photovoltage data taken from Ref. [12]; ΔCPD = change in contact potential difference).

(cleaved perpendicular to c-axis) in a basic aqueous electrolyte (curve 1), as well as surface photovoltage spectra (curves 2 and 3) reported by Brillson [12] for oxygen-adsorbed (70% coverage) and vacuum-cleaved (LEED-ordered) single crystal n-CdSe surfaces. Three capacitance increases/plateaux, associated with transitions from donor states at 1.04, 1.28 and 1.34 eV to the conduction band, are evident. Note that there is also a barely discernible capacitance decrease at ~1.6 eV, which corresponds to a transition from the valence band to an ionized donor state located just below the conduction band; this state occurs in much higher concentrations in some polycrystalline materials.

The similarity between the surface photovoltage spectrum for the oxygen-adsorbed surface and the EPS spectrum is striking, indicating that the surface oxide structure is similar in the two environments and that the same bandgap states are involved. The 1.04 eV transition, and possibly the transition at 1.28 eV (not resolved by the vacuum technique), must involve interface states associated with oxygen adsorption since no change in surface photovoltage was observed for the vacuum-cleaved CdSe (curve 3) in this energy range. The 1.34 eV transition is apparently intrinsic to CdSe since it is evident in the photovoltage spectra for both vacuum-cleaved and oxygen-adsorbed CdSe crystals. EPS data for n-CdSe single crystals with various surface pretreatments also indicate that both the 1.04 and 1.34 eV transitions are associated with interface states. For example, although the same transitions are observed in all cases, concentrations of the 1.04 and 1.34 eV states are reduced by photoetching and greatly increased by mechanical polishing. EPS data for n-CdSe in aqueous solutions also correlate extremely well with other solid-state literature data for oxygen-adsorbed surfaces (e.g., [13]). As an indica-

tion of the sensitivity of the EPS method, the concentration of the 1.04 eV interface state calculated according to Eq. (2) from the data in Fig. 8 is $3 \times 10^{12}/cm^2$, and that of the 1.28 eV state is $5 \times 10^{11}/cm^2$.

Amorphous Silicon

EPS has also been applied successfully to characterization of amorphous silicon. Figure 9 shows an EPS spectrum on three different scales (offset) for

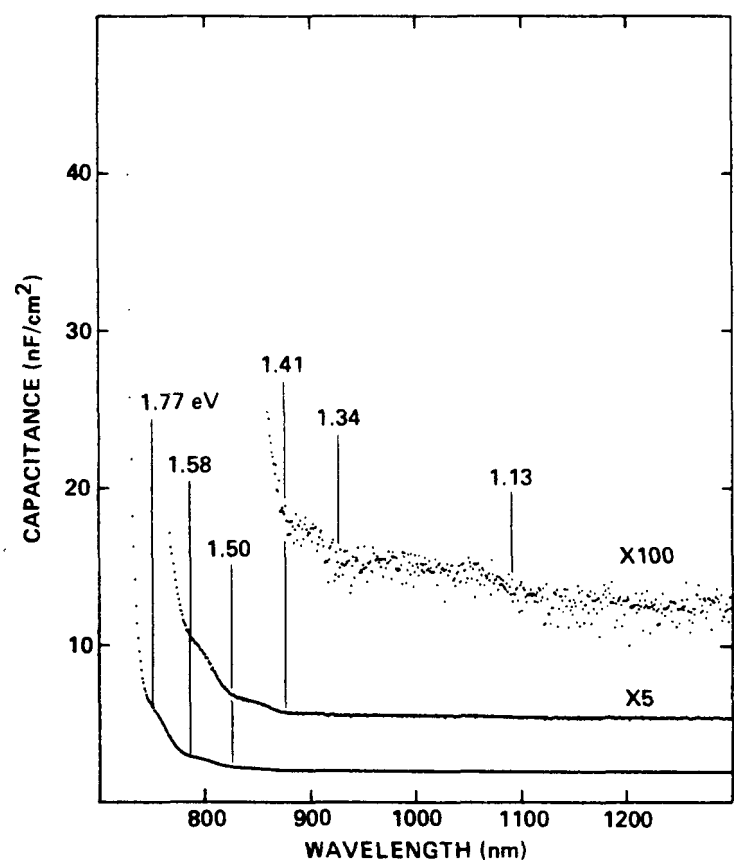

Fig. 9 EPS spectrum for a-Si (measured at 10 kHz) in 0.1 M tetrabutylammonium perchlorate/acetonitrile.

an a-Si specimen (deposited on stainless steel) in an acetonitrile electrolyte. Two relatively weak transitions (onsets at 1.13 and 1.34 eV) and four stronger transitions (onsets at 1.41, 1.50, 1.58 and 1.77 eV) are resolved as a series of plateaux, all corresponding to excitations from states within the mobility gap to the conduction band. Apparently, both band-tail states and gap states [14] in a-Si can be detected by EPS.

Kinetic Studies

Finally, EPS evaluation of deep level kinetic parameters will be illustrated for one specific case. Figure 10 shows a typical EPS spectrum obtained for thin-film p-Zn_3P_2 (prepared by chemical vapor deposition on tungsten coated silicon steel). Note that at wavelengths longer than 1100 nm the capacitance scale is 100-fold more sensitive and the EPS curve is offset. There are two well-defined peaks (0.74 and 1.02 eV) presumably corresponding to localized impurity transitions, and two capacitance increases (onsets at 1.08 and 1.27 eV) corresponding to transitions from the valance band to bandgap states. The 1.08 eV level is apparently an interface state since it varies considerably with surface pretreatment, sometimes obscuring the 1.02 eV peak. The other states apparently reside in the bulk.

Consider the 0.74 eV bulk state in p-Zn_3P_2. The time dependence of the photocapacitance after initiation and interruption of 1680 nm illumination is shown in Fig. 11. Figure 12 shows a plot of $\ln [(C_o^2 - C_t^2)/(C_o^2 - C_{t=0}^2)]$ vs time in the dark, which according to Eq. (25) should yield a straight line of slope k_n. The good linearity at longer times is evident. Note that the initial rapid decrease in C, which results in a non-zero intercept, is probably caused by edge

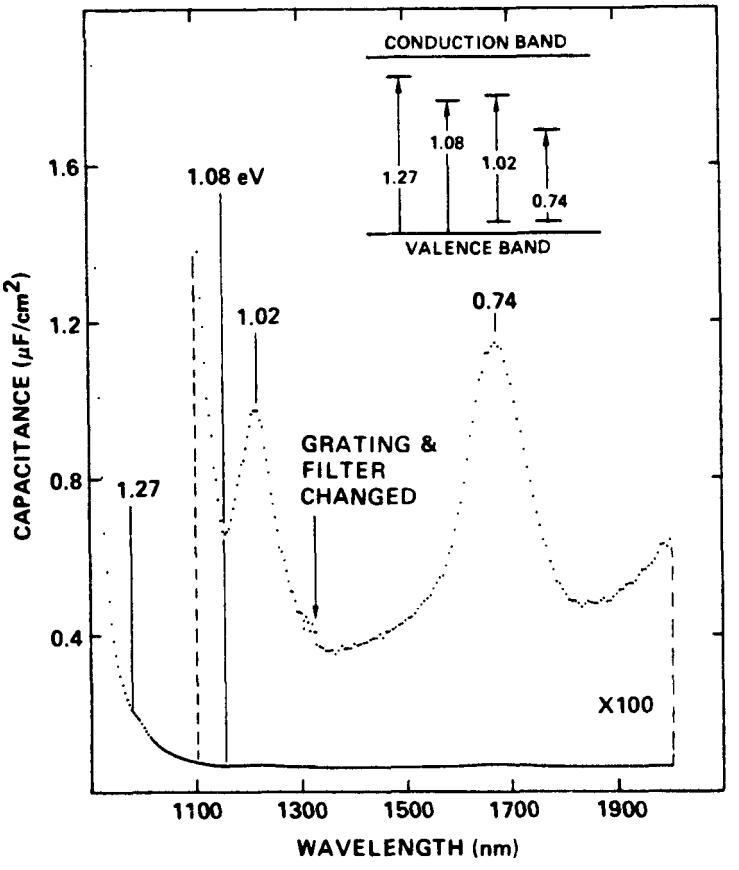

Fig. 10 EPS spectrum (measured at 5 kHz) for thin-film p-Zn_3P_2 (0.3 V vs U_{fb}) in 0.1 M tetrabutylammonium perchlorate/acetonitrile.

effects. Figure 13 shows the photocapacitance rise data from Fig. 11 and the theoretical curve (solid line) obtained by computer fitting the data to Eq. (27) using the k_n value from Fig. 12; the good fit is evident. Calculated values for N_s and k_o are also given in the figure. The value for N_s ($1.4 \times 10^{16}/cm^3$) is slightly higher than that calculated from the overall capacitance change ($8.5 \times$

$10^{15}/cm^3$) since trap saturation had not been attained. In cases for which the capacitance change is independent of illumination intensity, the two calculated values for N_s are found to be equivalent.

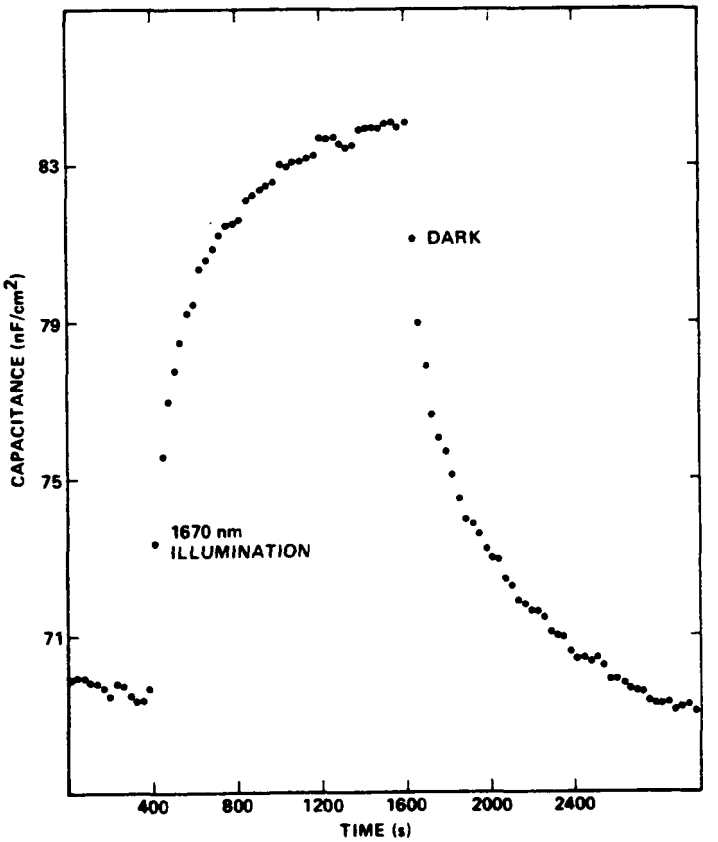

Fig. 11 Photocapacitance time dependence for the 0.74 eV state in thin-film p-Zn_3P_2 after initiation and interruption of 1680 nm illumination (conditions same as for Fig. 10).

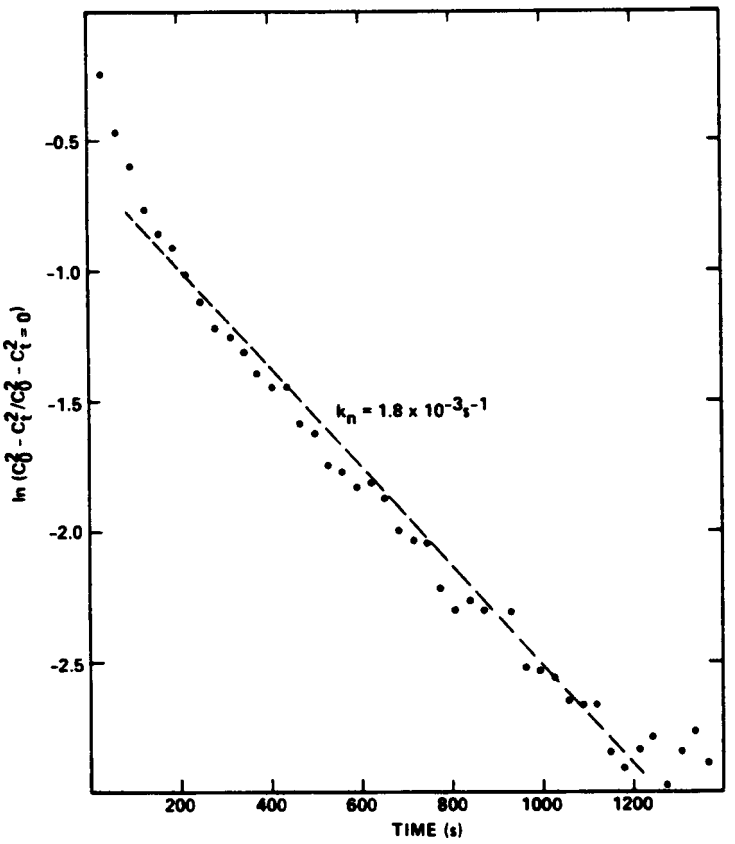

Fig. 12 Decay plot according to Eq. (25) for the data in Fig. 11.

SUMMARY AND CONCLUSIONS

Electrochemical photocapacitance spectroscopy has been demonstrated to be an extremely sensitive means for characterization of deep electronic levels in a wide variety of semiconductor materials. Application of the method, which is nondestructive and provides *in situ* electrochemical information, is

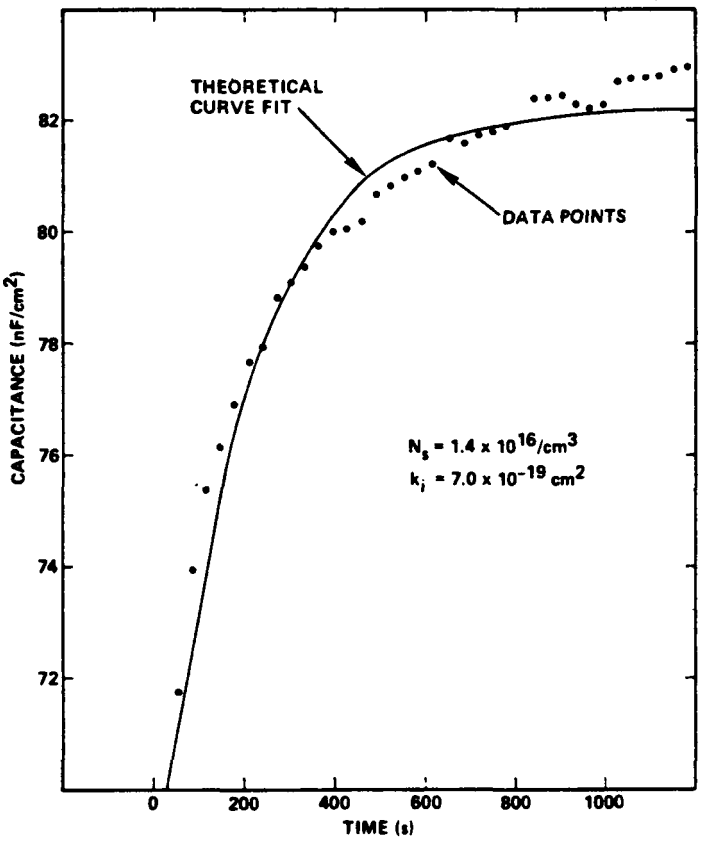

Fig. 13 Computer fit to the photocapacitance rise data in Fig. 11 and calculated N_s and k_0 values according to Eq. (27) for a bulk state.

relatively straightforward and rapid - the blocking contact is formed simply by immersing the semiconductor in a liquid electrolyte and measurements are made at ambient temperature and pressure. Information concerning the energetic location, density, and population/depopulation kinetics for both bulk and interface states is provided.

ACKNOWLEDGEMENTS

This work was partially supported by the Solar Energy Research Institute under Subcontract No. XG-0-9276. The authors thank Dr. Thomas McMahon of the Solar Energy Research Institute and Dr. Ting Chiu of Southern Methodist University for providing the a-Si and Zn_3P_2 specimens, respectively. The authors are also indebted to Dr. Kenneth Elliott, who provided the GaAs specimens and performed the DLTS measurements, and Dr. William Southwell, who provided the curve-fitting program used in the transient analyses. The surface photovoltage data in Fig. 8 were reproduced with permission of the publisher, North Holland Publishing Company, Amsterdam.

REFERENCES

1. R. Haak, C. Ogden and D. Tench, J. Electrochem. Soc. 129, 891 (1982).
2. N. F. Mott, Proc. R. Soc. London Ser. A 171, 27 (1939).
3. W. Schottky, Z. Phys. 118, 539 (1942).
4. J. O'M. Bockris and A. K. N. Reddy, Modern Electrochemistry, Vol. 2, Plenum Press, New York, p. 754, 1970.
5. G. L. Miller, D. V. Lange and L. C. Kimmerling, Ann. Rev. Mater. Sci. 7, 377 (1977).
6. C. H. Henry, H. Kukimoto, G. L. Miller and F. R. Merritt, Phys. Rev. B 7, 2499 (1973).
7. D.V. Lang and R.A. Logan, J. Appl. Phys. 47, 1533 (1976).

8. A. Mitonneau, G.M. Martin and A. Mircea, Electronics Lett. 13, 666 (1977).

9. A. Ashby, G.G. Roberts, D.J. Ashen and J.B. Mullin, Solid-State Commun. 20, 61 (1976).

10. G.M. Martin, A. Mitonneau and A. Mircea, Electronics Lett. 13, 191 (1977).

11. D. Bois, J. Physique 35, C3-241 (1974).

12. L.J. Brillson, Surf. Sci. 69, 62 (1977).

13. J.E. Ture, G.J. Russell and J. Woods, J. Cryst. Growth 59, 223 (1982).

14. R.A. Gibson, P.G. LeComber and W.E. Spear, Solid-State Electron. Devices 2, 53 (1978).